Journal of Cosmology, Vol. 27, No. 6, pp 18300 – 18354

Time Dilation Cosmology 10: Black Holes, Eternally Collapsing Objects, and the MECO Limit

Capt. Joseph H. (Cass) Forrington
captcass@captcass.com

Abstract

Time Dilation Cosmology (TDC) describes gravitational fields through a local time-rate factor and its associated differential relative to a distant reference observer. This paper applies that formulation to relativistic gravitational collapse and compares the resulting equations with the Eternally Collapsing Object (ECO) relations developed by Abhas Mitra and the Magnetospheric Eternally Collapsing Object (MECO) extension developed by Robertson and Leiter. Beginning from the shared spherical compactness relation stated explicitly in Section 2, the TDC time-rate formulation then derives the compactness bound, gravitational-redshift relation, relativistic enhancement of the local Eddington luminosity, redshift suppression of luminosity at infinity, and mass-energy depletion timescale. These relations are shown to be algebraically identical to the corresponding principal ECO relations under the exact mapping between gravitational redshift and the TDC local time-rate factor. The analysis is then extended beyond the static correspondence by allowing gravitational mass, radius, and time rate to evolve simultaneously. The resulting coupled dimensionless system exhibits an asymptotic attracting trajectory: numerical integrations beginning on both sides of the candidate relation converge toward $\frac{\varepsilon}{x^2} = 1$. Along this trajectory, radius, gravitational mass, and the local time-rate factor decrease asymptotically as ${t_\infty}^{-1}$, while gravitational redshift satisfies $1 + z \propto t_\infty$. The limiting compactness $\frac{2GM}{Rc^2} \to 1$ is approached only as $t_\infty \to \infty$, while the object remains timelike at every finite stage. The resulting TDC compact-object solution therefore reproduces the principal mathematical and dynamical behavior of the ECO limit without assuming the disputed ECO no-trapped-surface argument. An intrinsic magnetic moment and external magnetosphere may be added consistently as a MECO extension, although a complete electromagnetic and plasma derivation lies beyond the present analysis. The result is a specific, testable model of asymptotically collapsing compact-object behavior whose modeled surface remains untrapped under the stated assumptions, while its global horizon status remains to be established by a full causal analysis. This conditional prediction distinguishes the proposed evolution from the conventional event-horizon interpretation.

Keywords: Time Dilation Cosmology (TDC); Gravitational Collapse; Eternally Collapsing Objects (ECO); Magnetospheric Eternally Collapsing Objects (MECO); Gravitational Time Dilation; Black Holes; Gravitational Redshift; Asymptotic Collapse; Compactness Limit; Horizonless Compact Objects.

1. Introduction

The conventional black-hole solution of general relativity describes sufficiently compact gravitational collapse in terms of trapped surfaces, an event horizon, and an interior region from which signals cannot propagate to a distant observer. The observational evidence for extremely compact massive objects is extensive, but the physical interpretation of their limiting state remains a subject on which alternative relativistic constructions have been proposed. The present paper examines that limiting state within Time Dilation Cosmology (TDC), with particular attention to whether, after the shared spherical compactness input is specified, the TDC time-rate formulation produces the mathematical behavior previously associated with Eternally Collapsing Objects (ECOs) and Magnetospheric Eternally Collapsing Objects (MECOs).

An earlier TDC treatment of compact objects proposed that the object conventionally identified as a black hole is better described as an extreme spacetime vortex in which the local rate of time becomes progressively attenuated toward the focus [1]. In that interpretation, increasing gravitational time dilation causes

frequencies and apparent motion to decrease for a distant observer, while energy associated with the highly stressed spacetime/electromagnetic field may be retained and subsequently emitted. That earlier treatment was primarily physical and geometrical. It did not develop a complete dynamical collapse calculation or compare the resulting equations with an independently developed relativistic collapse model.

Abhas Mitra developed an alternative treatment of continued spherical gravitational collapse in which a material configuration remains timelike and does not form a finite-mass trapped surface. In this formulation, continued collapse approaches an ECO limiting state characterized by increasing gravitational redshift, decreasing gravitational mass, and an asymptotic compactness approaching the Schwarzschild limit while the limiting state is never attained in finite evolution [2,3]. Mitra subsequently developed the radiation-pressure-supported ECO interpretation in which the local Eddington luminosity increases with gravitational redshift while the luminosity measured by a distant observer is correspondingly reduced [3]. These conclusions are not the standard interpretation of gravitational collapse in general relativity, and the present analysis does not assume the validity of Mitra's disputed no-trapped-surface argument. Instead, his equations are used as an independent mathematical comparison against which the TDC derivation can be evaluated.

Robertson and Leiter extended the ECO concept to the Magnetospheric Eternally Collapsing Object (MECO), incorporating an intrinsic magnetic moment, an Eddington-regulated radiating surface, a pair-plasma atmosphere, and extreme gravitational redshift [4]. The MECO construction was proposed as an alternative description of galactic black-hole candidates and active galactic nuclei. The distinction between ECO and MECO is retained throughout the present paper: ECO refers principally to the relativistic collapse and radiation-supported limiting behavior developed by Mitra, whereas MECO refers to the magnetospheric extension developed by Robertson and Leiter.

The purpose of the present paper is not to import the ECO or MECO assumptions into TDC. It is to determine, step by step, which corresponding relations follow from the TDC time-rate field after the shared spherical compactness input is specified. For this reason, the mathematical development is presented in paired form. At each major stage, the relevant Mitra relation is stated first, with its original source and equation number where available, followed immediately by the corresponding TDC derivation. This arrangement permits the compactness condition, gravitational redshift, mass-radius behavior, local Eddington luminosity, luminosity at infinity, mass-depletion timescale, and asymptotic collapse behavior to be compared directly.

Because the comparison introduces variables from both formalisms, all quantities are explicitly defined when first used. In particular, the analysis distinguishes the TDC local time-rate factor, the TDC time-rate differential, gravitational mass, areal radius, compactness, gravitational redshift, local and distant-observer luminosities, opacity, local proper time, distant-observer time, and the radial variables used in Mitra's collapse formalism. Symbols that acquire a specialized meaning in either formulation are not assumed to be interchangeable unless the equivalence is explicitly derived.

The analysis first establishes the TDC compactness relation and its allowed domain. It then derives the reciprocal temporal and radial spatial factors, the gravitational time-rate gradient, the local Eddington balance, the redshift transformation of luminosity, and the mass-loss timescale. The resulting equations are compared directly with the corresponding ECO relations. The treatment is then extended beyond a static compactness comparison by allowing both gravitational mass and radius to evolve. This produces a coupled TDC collapse system whose asymptotic behavior can be tested for convergence toward an ECO-like limiting state.

The distinction between established gravitational relations and the new results of the present analysis is essential. The spherical compactness relation, its associated gravitational redshift, and the standard transformations of photon energy and luminosity are not claimed as new predictions of TDC. Their

reproduction establishes the mathematical correspondence between the TDC time-rate parameterization and the conventional spherical gravitational description. The additional contribution of TDC 10 lies in the specified coupling of gravitational mass loss, radial contraction, and the evolving local time-rate field. Under the stated radiative and contraction assumptions, this coupling produces a dynamical system whose trajectories can be examined for convergence toward an asymptotic compactness limit. The resulting mass-radius-time evolution, its stability, and its dependence on the contraction prescription constitute the principal model-specific results investigated here. Whether this limiting behavior describes a physically realized horizonless object requires additional consideration of the dynamical spacetime and its causal structure.

The central question is whether, given the shared spherical compactness relation, the TDC time-rate formulation reproduces ECO relations and yields additional predictions from its coupled dynamical equations.

2. Definitions and Mathematical Framework

Because this paper compares two formalisms that use different variables for closely related physical quantities, the notation is fixed before the comparison is developed. A symbol is not treated as equivalent in the Mitra/ECO and TDC formulations merely because the two expressions have a similar form. Equivalence will be asserted only where it is derived explicitly in a later section. Unless otherwise stated, the compact object is treated as spherically symmetric, R denotes areal (circumference) radius, M denotes gravitational mass enclosed within that radius, and G and c have their usual meanings.

2.1 TDC Time-Rate Variables

The central TDC quantity used in this paper is the local time-rate factor T_o. It is the rate of local proper time relative to the time increment assigned by a distant reference observer:

$$T_o = d\tau / dt_\infty \tag{1}$$

Here, $d\tau$ is the infinitesimal proper-time interval measured locally with the material element, and dt_∞ is the corresponding infinitesimal time interval for the distant reference observer. Thus $T_o = 1$ represents no gravitational time-rate attenuation relative to that reference, whereas $T_o \to 0$ represents the limiting case in which the local evolution appears increasingly slowed to the distant observer.

The observer convention used throughout this paper is therefore explicit: t_∞ is the time assigned by an asymptotically distant reference observer, while τ is the proper time of the local material element. The boundary condition is $T_o \to 1$ as $R \to \infty$, so that $dR_t \to 0$ in the same limit.

TDC expresses the departure from the invariant reference rate through the time-rate differential dR_t, defined by

$$dR_t = 1 - T_o \tag{2}$$

Accordingly, $dR_t = 0$ corresponds to $T_o = 1$, while $dR_t \to 1$ corresponds to $T_o \to 0$. In the spherical gravitational comparison developed here, the TDC time-rate factor is written

$$T_o = \sqrt{(1 - 2GM / Rc^2)} \quad (3)$$

where M is the gravitational mass enclosed by the surface of areal radius R. Equation (3) is used only in the spherical compact-object regime considered in this paper; it is not introduced as a general definition of T_o for arbitrary geometries.

Equation (3) supplies the standard spherical compactness factor used as the temporal input to the present TDC compact-object treatment. The subsequent TDC relations are derived from this time-rate formulation without importing Mitra's ECO dynamical equations or his disputed inference concerning trapped-surface formation. In this paper, therefore, "independent TDC derivation" means independent derivation after this common spherical compactness input, not the absence of any shared spherical gravitational relation.

For convenience, define the dimensionless compactness parameter C by

$$C = 2GM / Rc^2 \quad (4)$$

Equations (2)-(4) then imply

$$C = 1 - T_o^2 = 2dR_t - dR_t^2 \quad (5)$$

The quantity C will be used repeatedly because C = 1 identifies the limiting Schwarzschild compactness. No conclusion concerning the formation or non-formation of a trapped surface is assumed at this stage; the allowed domain and its consequences are derived in the following section.

2.2 Gravitational Redshift and Reciprocal Radial Scaling

The gravitational redshift is defined through the ratio of locally emitted to distantly observed photon frequency. For the spherical relation of Equation (3),

$$1 + z = 1 / T_o \quad (6)$$

Thus z is the gravitational redshift measured relative to the distant reference observer. The limit $T_o \to 0$ is equivalently $z \to \infty$.

The symbol $d\ell$ denotes an infinitesimal local proper radial distance. The coordinate increment dR denotes the corresponding change in areal radius. Proper radial distance and areal-radius change are not generally interchangeable in a strong gravitational field.

The relation between them follows from the reciprocal time-space scaling previously developed in TDC 5. There, preservation of the invariant speed of light is used to establish the TDC principle that when an observed rate of time is reduced, the corresponding observed spatial scale increases in reciprocal proportion; conversely, a faster observed time rate corresponds to spatial compression [5]. In the notation of the present paper, the radial spatial scale factor relative to the distant reference is therefore

$$S_r = 1 / T_o \quad (7)$$

where S_r is the radial spatial scale factor. Applying that factor to an areal-radius coordinate increment gives

$$d\ell = S_r\, dR \tag{8}$$

and substitution of Equation (7) yields

$$d\ell = dR / T_o \tag{9}$$

or equivalently

$$dR = T_o\, d\ell \tag{10}$$

Thus Equation (9) is not introduced as an independent geometric assumption in TDC 10. It is the spherical radial application of the reciprocal temporal-spatial scaling already stated in TDC 5. The present paper makes that application explicit so that the proper-distance relation used later in the contraction dynamics is mathematically defined rather than assumed [5].

Combining Equation (9) with Equation (3) gives

$$d\ell^2 = dR^2 / T_o^2 = dR^2 / (1 - 2GM/Rc^2) \tag{11}$$

The corresponding effective spherical line element used for the temporal and radial sectors of the present calculation may therefore be written

$$ds^2 = -T_o^2 c^2 dt_\infty^2 + dR^2/T_o^2 + R^2 d\Omega^2 \tag{12}$$

with $T_o^2 = 1 - 2GM/(Rc^2)$ and where, $d\Omega^2 = d\theta^2 + \sin^2\theta d\phi^2$ is the differential solid-angle element, where θ and ϕ are the polar and azimuthal angular coordinates, respectively. Equation (12) states explicitly the spherical temporal and radial geometry used in the TDC compact-object calculation. It is not presented as a new generally covariant set of TDC field equations for arbitrary spacetime geometries. During radiative evolution, its use is quasi-static: the instantaneous M and R determine the surface time-rate and radial factors at each stage. The exterior time-dependent spacetime and the conditions under which this quasi-static treatment is applied are specified in the later dynamical section.

2.2.1 Geometric status of the reciprocal scaling and exterior metric

The reciprocal radial relation $d\ell = dR/T_o$ is adopted here as the radial spatial prescription of the TDC model, motivated by the reciprocal time–space scaling discussed in TDC 5. In the present manuscript it is not derived from an independently specified covariant TDC field equation. Preservation of the locally measured speed of light alone does not uniquely determine a radial metric coefficient without additional assumptions concerning the coordinate definitions and spacetime geometry.

The areal radius R is operationally defined by the area $4\pi R^2$ of a symmetry sphere; $d\ell$ is the proper radial separation along a constant-time spatial slice of the specified static exterior geometry. Consequently, $d\ell = dR/T_o$ is not a change of radial coordinate or a statement that the areal radius itself is a proper-distance coordinate. The identification fixes the radial metric coefficient for the chosen static, spherical slicing.

With $T_o^2 = 1 - 2GM/(Rc^2)$, Equation (12) is exactly the Schwarzschild exterior line element in standard areal-radius coordinates for constant M and $R > 2GM/c^2$. It therefore has the same invariant curvature as Schwarzschild in that domain; in particular, its vacuum Ricci scalar vanishes and its Kretschmann scalar is $48G^2M^2/(c^4R^6)$. No distinct static-exterior curvature invariant is claimed. This metric is a vacuum solution of the Einstein field equations in that static domain, but this observation does not derive a separate TDC gravitational field theory.

The novel, model-dependent proposal examined below is instead the prescribed evolution of the surface mass, radius, and time-rate factor under radiative loss and contraction. The instantaneous Schwarzschild form is used quasi-statically at the surface; it must not be interpreted as an exact global solution for a time-dependent radiating exterior. The outgoing Vaidya exterior and matching assumptions are discussed in Section 7. The present treatment is accordingly a TDC time-rate parametrization and conditional dynamical compact-object model, not a completed alternative covariant theory of gravity.

2.2.2 Operational radius, proper distance, and coordinate status

The areal radius R is defined by the invariant area of each symmetry two-sphere, $A_s = 4\pi R^2$, or equivalently by its circumference $2\pi R$. This definition does not require a radial ruler extending from the center and remains distinct from the proper distance between neighboring spheres. In the static exterior used in Equation (12), an observer at fixed R is stationary relative to the asymptotic time coordinate; the radial proper distance $d\ell$ between adjacent stationary observers is measured along the constant-t_∞ spatial slice, giving $d\ell^2 = g_{RR}\, dR^2$ and $d\ell = dR/T_o$ on the positive exterior branch.

The factor $S_r = 1/T_o$ is therefore the ratio of a proper radial increment on that specified slice to the corresponding areal-radius increment. It is not the Jacobian of an arbitrary coordinate relabeling. One can introduce a proper-distance coordinate ℓ by integrating $d\ell = dR/T_o$ for a static mass parameter, but that coordinate change does not alter the geometry or its curvature invariants, and the angular area remains $4\pi R(\ell)^2$. In particular, replacing R by ℓ in the angular term as though ℓ were an areal radius would describe a different metric.

The logical status of the construction is important. TDC adopts the reciprocal temporal–radial prescription $S_r = 1/T_o$ and combines it with the shared spherical compactness relation to specify Equation (12). Once that line element is specified, the proper-distance formula also follows from its radial metric coefficient; this is a consistency check, not a separate derivation of the prescription from gravitational field equations. As noted in Section 2.2.1, for constant M this is the Schwarzschild exterior expressed in areal-radius coordinates, not a geometrically distinct static solution.

Finally, radial proper distance is slicing-dependent: $d\ell = dR/T_o$ refers to the static exterior foliation and is not an invariant separation between arbitrary events or freely falling observers. During the radiative evolution of Sections 7–9, its use at the moving surface is an instantaneous quasi-static approximation. A fully time-dependent interior–exterior geometry would require an explicit choice of spacelike slicing and a corresponding local radial metric before the same conversion could be asserted beyond that approximation.

2.3 Mitra/ECO Collapse Variables

For comparison with Mitra's spherical-collapse formulation, this paper retains his principal radial variables U, Γ, and V. In the notation used by Mitra, U is the rate of change of areal radius along the proper time of a comoving fluid element,

$$U = dR / d\tau \tag{13}$$

The quantity Γ is defined as the change in areal radius with local proper radial distance,

$$\Gamma = dR / d\ell \tag{14}$$

Mitra further defines the local radial three-speed variable V by

$$V = U / \Gamma \tag{15}$$

and uses the relation

$$U = \Gamma V \tag{16}$$

In Mitra's 2002 treatment these definitions lead to the spherical-collapse identity, in units G = c = 1,

$$\Gamma^2 = 1 + U^2 - 2M/R \tag{17}$$

and, after substitution of Equation (16), to

$$\Gamma^2(1 - V^2) = 1 - 2M/R \tag{18}$$

Equations (13)-(18) are presented here to define the notation used in the subsequent side-by-side comparison; they are Mitra/ECO relations and are not assigned as TDC results. Mitra's inference from Equation (18) that trapped surfaces cannot form has been disputed. TDC 10 therefore does not assume that inference. Instead, the TDC compactness domain will be derived from the TDC time-rate domain and only then compared with Mitra's result [2].

When SI units are restored, dimensionless velocity factors such as V^2 in Equation (18) are understood as V^2/c^2, and $2M/R$ becomes $2GM/(Rc^2)$. This paper will normally retain G and c explicitly in the TDC equations so that dimensional consistency remains visible.

2.4 Radiation and Mass-Energy Variables

The symbol κ denotes the effective opacity of the radiating material, with dimensions of area per unit mass. L_{loc} denotes luminosity measured locally at the radiating surface, while L_∞ denotes luminosity received by a distant observer. Their Eddington-limited values are denoted $L_{Edd,loc}$ and $L_{Edd,\infty}$, respectively.

The local radiative flux at areal radius R is

$$F_{rad} = L_{loc} / (4\pi R^2) \tag{19}$$

For opacity κ, the standard local radiation-force acceleration used in the Eddington balance is

$$a_{rad} = \kappa F_{rad} / c \tag{20}$$

Equation (20) is standard radiation physics rather than a new TDC postulate. The relativistic gravitational factor entering the corresponding Eddington balance will, however, be derived from the TDC time-rate gradient rather than inserted from the ECO result.

The gravitational mass is allowed to evolve during radiative collapse. A dot over a quantity will denote differentiation with respect to distant-observer time unless another time variable is explicitly stated:

$$\dot{M} = dM / dt_\infty \tag{21}$$

For outward radiation carrying positive energy to infinity, L_∞ corresponds to $-\dot{M}$ through mass-energy conservation,

$$L_\infty = -c^2\dot{M} \tag{22}$$

2.5 Departure from the Limiting Compactness

For the dynamical analysis it is useful to define a nonnegative departure parameter ε by

$$\varepsilon = 1 - 2GM/(Rc^2) \tag{23}$$

Using Equation (3),

$$\varepsilon = T_o^2 \tag{24}$$

Thus ε measures the distance, in compactness space, from the limiting value $2GM/(Rc^2) = 1$. The asymptotic limit examined later in the paper is

$$\varepsilon \to 0^+ \tag{25}$$

which is equivalent to $T_o \to 0^+$, $dR_t \to 1^-$, $z \to \infty$, and $2GM/(Rc^2) \to 1^-$.

Finally, when a local proper inward contraction speed is required in the TDC dynamical treatment, it will be denoted by u and defined by

$$u = -d\ell / d\tau \tag{26}$$

The explicit minus sign makes u positive for inward contraction. This is a TDC dynamical variable introduced for the present analysis and should not be confused with Mitra's U.

2.6 Comparison Convention

In Sections 3–7, ECO relations are identified by source and compared with the corresponding TDC derivations. Quoted ECO equations retain their source identification; equations used in the TDC development follow the manuscript's numbered sequence.

The comparison distinguishes quoted ECO relations, standard physical laws, and results obtained from the TDC time-rate formulation under the stated spherical compactness input.

Source verification: Mitra's 2006 luminosity-redshift and depletion-time formulas are identified as Equations (42) and (43), respectively, in the published 2006 article [3]. The 2002 spherical-collapse identities are attributed to Mitra [2], but no original equation number is asserted here for them because an equation-by-equation comparison against the full typeset 2002 article has not been completed. The TDC equation numbers throughout are the independent sequence of the present manuscript.

3. Compactness and the Trapped-Surface Limit

The first comparison concerns the compactness of a spherically collapsing body and the condition associated with formation of a trapped surface.

As established explicitly in Section 2, the two descriptions are not completely independent at their starting point: both employ the same spherical compactness factor $1 - 2GM/(Rc^2)$. The question addressed here is narrower and more precise. Given that common spherical input, does the TDC time-rate formulation, without importing Mitra's collapse equations or his disputed no-trapped-surface inference, impose the same finite-state compactness bound?

3.1 Mitra's collapse relation

For a spherically symmetric collapsing fluid, Mitra employs the Misner–Sharp variables U and Γ. In the notation defined in Section 2, U is the rate of change of areal radius with respect to the comoving proper time τ, Γ relates the areal-radius gradient to proper radial distance, and V is the locally measured radial three-velocity. The collapse equations may be combined in the form

$\Gamma^2(1 - V^2/c^2) = 1 - 2GM/(Rc^2)$ Mitra relation

Here G is Newton's gravitational constant, M is the gravitational mass contained within areal radius R, c is the invariant speed of light, Γ is Mitra's radial derivative factor, and V is the locally measured radial velocity of the collapsing matter. Mitra interprets the non-negativity of the left-hand side for causal material motion as requiring

$2GM/(Rc^2) \leq 1$ Mitra compactness condition.

Mitra consequently argues that trapped surfaces, which require $2GM/(Rc^2) > 1$ in this formulation, do not form during physical spherical collapse. This conclusion is a disputed interpretation of general relativity and is not assumed in the TDC analysis below.

The purpose of the comparison is instead to determine whether, after the shared spherical compactness factor has been specified, the independent TDC time-rate domain produces the same bound without using Mitra's Γ–V argument.

3.2 TDC compactness relation

TDC begins with the gravitational time-rate factor T_o, defined in Section 2 as the local rate of time relative to the distant reference rate. For the spherically symmetric gravitational field considered here, Section 2 gives

$$T_o = \sqrt{(1 - 2GM/Rc^2)} \quad (27)$$

where T_o is dimensionless. Equation (27) is the common spherical compactness input identified in Section 2; it is not claimed here as a relation derived independently of the Schwarzschild compactness factor.

TDC independently parameterizes this spherical relation through its time-rate differential dR_t, defined by

$$dR_t = 1 - T_o \quad (28)$$

so that

$$T_o = 1 - dR_t \quad (29)$$

Substitution of Equation (29) into Equation (27), followed by squaring, gives

$$(1 - dR_t)^2 = 1 - 2GM/Rc^2 \quad (30)$$

and rearranging yields the TDC compactness identity

$$2GM/Rc^2 = 2dR_t - dR_t^2 \quad (31)$$

Equation (31) expresses the conventional dimensionless compactness entirely in terms of the TDC time-rate differential. The new content at this stage is therefore not the spherical compactness factor itself, but its parameterization and allowed domain in the TDC time-rate variables.

3.3 TDC domain and the compactness bound

For a finite timelike material state in TDC, the local time-rate factor remains positive:

$$T_o > 0 \quad (32)$$

and therefore

$$0 \leq dR_t < 1 \quad (33)$$

Substitution of this domain into Equation (31) gives

$$0 \leq 2dR_t - dR_t^2 < 1 \quad (34)$$

and hence, for every finite timelike state,

$$2GM/Rc^2 < 1 \quad (35)$$

The limiting value is approached as the local time rate tends to zero:

$$T_o \to 0^+ \Leftrightarrow dR_t \to 1^- \Leftrightarrow 2GM/Rc^2 \to 1^- \quad (36)$$

Thus, within the TDC formulation, the finite-state compactness restriction follows from the permitted domain of the TDC time-rate variable once the spherical compactness relation of Equation (27) has been specified. It does not require Mitra's inference from Γ and V. The numerical limiting condition is the same, but the additional premise used to obtain the finite-state restriction is different.

3.4 Direct comparison

The correspondence can now be stated directly. Mitra's collapse relation contains the compactness factor

$1 - 2GM/(Rc^2)$ Mitra compactness factor.

whereas TDC identifies the same factor as

$$1 - 2GM/Rc^2 = T_o{}^2 = (1 - dR_t)^2 \quad (37)$$

Consequently, Mitra's dynamical relation may be written in TDC variables as

$$\Gamma^2(1 - V^2/c^2) = T_o{}^2 = (1 - dR_t)^2 \quad (38)$$

This equation is a mapping between the two descriptions, not an assertion that Γ, V, and dR_t are identical physical quantities. Γ and V are variables in Mitra's relativistic collapse formulation; T_o and dR_t are TDC time-rate variables. What is common to the two formulations is the spherical compactness factor that relates them.

If γ_v denotes the Lorentz factor associated with V,

$$\gamma_v = 1/\sqrt{(1 - V^2/c^2)} \quad (39)$$

then Equation (38) gives, on the positive branch,

$$\Gamma = \gamma_v T_o \quad (40)$$

where γ_v is dimensionless. In the static limit V = 0, $\gamma_v = 1$, and Equation (40) reduces to $\Gamma = T_o$. The dynamical relation therefore contains the TDC time-rate factor multiplied by the Lorentz factor associated with the local radial motion.

3.5 Consequence for the limiting mass-radius relation

Equation (35) can also be written as a mass-radius bound:

$$M < Rc^2/(2G) \quad (41)$$

For continued collapse that remains within the TDC timelike domain, if the areal radius approaches zero, the upper bound on M approaches zero. With non-negative gravitational mass,

$$R \to 0 \Rightarrow M \to 0 \quad (42)$$

In the limiting state described by Equation (36), Equation (31) gives

$$2GM/(Rc^2) \to 1 \quad (43)$$

while both M and R may tend asymptotically to zero. Thus TDC admits the limiting set

$$M \to 0, \quad R \to 0, \quad 2GM/(Rc^2) \to 1 \tag{44}$$

Mitra likewise associates continued spherical collapse with M approaching zero and the compactness approaching its limiting value. The correspondence established here is substantive, but it should not be described as a proof of Mitra's broader claim that general relativity itself prohibits trapped-surface formation.

More precisely, the TDC result is conditional on the spherical time-rate relation stated in Section 2 and on the TDC requirement $T_o > 0$ for every finite timelike material state. Under those premises, the compactness remains below unity at every finite state and can approach unity only as T_o approaches zero.

An important distinction must be made between a restriction imposed on the allowed TDC material states and a demonstration that gravitational collapse cannot produce trapped surfaces. The condition $T_o > 0$, together with the adopted spherical compactness relation, restricts the present TDC solution to configurations satisfying $2GM/(Rc^2) < 1$. It does not independently establish that an initially untrapped collapsing configuration must remain within this domain under unrestricted gravitational evolution. Such a conclusion requires examination of the coupled mass-radius dynamics and the causal properties of the evolving spacetime. Accordingly, the present result establishes the compactness domain of the proposed TDC solution, while the question of whether its dynamical evolution preserves that domain is examined in Sections 8 and 9.

3.5.1 Invariant trapped-surface criterion and limits of the surface calculation

In spherical symmetry, the invariant local criterion for a marginally trapped sphere is that the gradient of areal radius becomes null: $g^{ab}(\nabla_a R)(\nabla_\beta R) = 0$. With the Misner–Sharp mass definition, this scalar equals $1 - 2GM/(Rc^2)$. Its sign is positive on untrapped spheres, zero on marginal spheres, and negative on trapped spheres, subject to the orientation of the two null expansions. Equivalently, for future-directed outgoing and ingoing null normals, an ordinary untrapped sphere has positive outgoing expansion and negative ingoing expansion; a future trapped sphere has both expansions negative. The normalizations of individual expansions may vary, but their signs and vanishing are invariant under positive rescaling of the null normals.

For the adopted instantaneous exterior surface relation, $T_o^2 = 1 - 2GM/(Rc^2) > 0$ therefore places the modeled surface on the untrapped side of this local criterion at each stage for which the quasi-static approximation and assumed domain hold. This is a conditional statement about the modeled surface, not a proof that every spherical surface in the evolving spacetime is untrapped. In particular, the global event horizon is defined by causal accessibility of future null infinity and cannot be excluded by a positive surface time-rate factor at a sequence of finite times alone.

The numerical evolution in Sections 8–9 tests whether the prescribed mass-loss and contraction equations keep the surface compactness below unity over the integration domain. It does not independently establish a complete interior solution, the signs of both null expansions throughout the spacetime, or the global causal structure of the outgoing-radiation geometry. A proof that the proposed collapse remains horizonless would require an interior–exterior matched dynamical solution and null-geodesic or null-expansion analysis. Consequently, “horizonless” in this paper denotes the conditional surface behavior of the proposed model, not an established global no-event-horizon theorem.

3.6 Result

Both approaches yield the same limiting compactness factor. Mitra invokes his interpretation of Γ and V; TDC instead imposes the positive local time-rate domain after adopting the shared spherical relation.

This conditional compactness bound does not independently rule out trapped surfaces. Sections 8–9 examine whether the prescribed TDC mass–radius evolution preserves the domain and approaches the limit asymptotically.

3.6.1 Relation to established collapse results and alternative compact objects

Classical relativistic collapse provides a necessary point of comparison. The Oppenheimer–Snyder solution exhibits formation of a black-hole region in a pressureless spherical collapse model, with finite comoving proper time despite the familiar infinite-redshift appearance in distant Schwarzschild time [6]. Penrose's trapped-surface analysis establishes geodesic incompleteness under its specified global and energy conditions; it does not assert that every radiating stellar model forms a trapped surface [7]. These results cannot be displaced merely by requiring $T_o > 0$ at the modeled surface.

The present calculation differs in imposing an Eddington-regulated mass-loss law and a prescribed contraction speed while retaining a quasi-static surface compactness relation. Its numerical trajectories establish an untrapped modeled surface within that reduced system, not the global causal structure of a fully matched dynamical spacetime. Thus they do not refute the established collapse solutions or prove that a global event horizon is impossible. The relevant comparison is between distinct physical assumptions and their corresponding solutions, not a universal prohibition of black holes.

Horizonless alternatives are themselves diverse. For example, the gravitational-vacuum-condensate-star construction of Mazur and Mottola replaces the would-be horizon with a thin transition layer and a nonstandard interior equation of state [8]. That mechanism is distinct both from Mitra's radiative ECO proposal [2,3] and from the mass-loss/contraction closure investigated here. Demonstrating which alternative, if any, is realized astrophysically requires consistent interior–exterior dynamics and observational discrimination.

4. Gravitational Redshift and the TDC Time-Rate Limit

The compactness correspondence established in Section 3 leads directly to a second comparison: gravitational redshift. This quantity is especially useful because Mitra employs the surface redshift z as a measure of relativistic compactness, whereas TDC expresses the same physical limit through the local time-rate factor T_o and the time-rate differential dR_t.

Because the spherical compactness factor has already been identified as a common input, the purpose of this section is not to claim an independent derivation of the Schwarzschild redshift relation. It is to establish explicitly the mapping between the conventional redshift variable z and the TDC variables T_o and dR_t, using the observer convention defined in Section 2.

4.1 Mitra's gravitational-redshift relation

Mitra defines the gravitational redshift z at the surface of a spherical compact object by the standard Schwarzschild relation

$1 + z = [1 - 2GM/(Rc^2)]^{-1/2}$ Mitra gravitational-redshift relation.

Here z is the dimensionless gravitational redshift measured by a distant observer, M is the gravitational mass, R is the areal radius of the emitting surface, G is Newton's gravitational constant, and c is the invariant speed of light. Mitra uses this relation as the principal compactness parameter in the highly relativistic regime. In his ECO treatment, continued contraction toward the Schwarzschild compactness limit corresponds to

$z \to \infty$ Mitra ECO limiting redshift.

The significance of this limit in Mitra's model is that radiation emitted from the collapsing surface becomes increasingly redshifted and time-dilated as seen by a distant observer. His 2006 ECO analysis subsequently uses this same factor, 1 + z, in the local Eddington luminosity and in the observed collapse timescale.

4.2 Mapping the redshift factor to TDC variables

Section 2 defines the local gravitational time-rate factor relative to the distant observer as

$$T_o = d\tau/dt_\infty = \sqrt{(1 - 2GM/Rc^2)} \quad (45)$$

Taking the reciprocal gives

$$1/T_o = [1 - 2GM/(Rc^2)]^{-1/2} \quad (46)$$

Comparison with Mitra's redshift relation therefore gives

$$1 + z = 1/T_o \quad (47)$$

Using the TDC definition $T_o = 1 - dR_t$, Equation (47) becomes

$$1 + z = 1/(1 - dR_t) \quad (48)$$

or equivalently

$$z = dR_t/(1 - dR_t) \quad (49)$$

Equation (49) expresses gravitational redshift directly in terms of the TDC time-rate differential. The variables z and dR_t are dimensionless. As dR_t increases, the local rate of time T_o decreases and the redshift measured by the distant observer increases.

4.3 Inverse relation: time-rate differential as a function of redshift

For later comparisons it is useful to invert Equation (48):

$$T_o = 1/(1 + z) \quad (50)$$

and therefore

$$dR_t = z/(1 + z) \quad (51)$$

Thus a measured gravitational redshift may be translated directly into the corresponding TDC time-rate differential. In the weak-field limit $z \ll 1$, Equation (51) gives $dR_t \approx z$. In the strong-field limit, dR_t approaches its upper limiting value while z grows without bound.

4.4 Compactness correspondence

The compactness-redshift relation need not be re-derived at length here because Section 3 has already established the compactness identity. Combining Equation (47) with $T_o^2 = 1 - 2GM/(Rc^2)$ gives directly

$$2GM/(Rc^2) = 1 - 1/(1 + z)^2 \quad (52)$$

Accordingly,

$$z \to \infty \Leftrightarrow T_o \to 0 \Leftrightarrow dR_t \to 1 \Leftrightarrow C \to 1 \quad (53)$$

This compactness correspondence provides the basis for the luminosity analysis developed in the following sections.

4.5 Frequency and photon-energy shift

The physical meaning of the redshift relation can also be written directly in terms of frequency. Let ν_{loc} denote the photon frequency measured locally at the emitting surface and ν_∞ the frequency measured by a distant observer. Gravitational redshift gives

$$\nu_\infty = \nu_{loc}/(1 + z) \quad (54)$$

Using Equation (47),

$$\nu_\infty = T_o \nu_{loc} \quad (55)$$

where ν_{loc} and ν_∞ are measured in hertz. Since photon energy is $E = h\nu$, with h denoting Planck's constant, the same factor applies to the energy of an individual photon:

$$E_\infty = T_o E_{loc} \quad (56)$$

Equation (56) describes the energy measured by the distant observer, not destruction of locally conserved energy. It is the observed photon-energy shift associated with the difference between the local and distant time rates.

4.6 Time dilation

The same factor appears in the relation between local proper time τ and distant-observer time t_∞. From the observer convention defined in Section 2,

$$d\tau = T_o \, dt_\infty \quad (57)$$

and therefore

$$dt_\infty = d\tau/T_o = (1 + z)d\tau \quad (58)$$

Using the TDC variable,

$$dt_\infty = d\tau/(1 - dR_t) \quad (59)$$

Thus gravitational redshift and gravitational time dilation are not separate limiting parameters in this formulation. Both are determined by the same local time-rate factor T_o.

4.7 The limiting state

For every finite timelike state, Section 3 requires $dR_t < 1$ and $T_o > 0$. Consequently, z remains finite and the compactness remains below unity:

$$0 < T_o \leq 1 \Leftrightarrow 0 \leq dR_t < 1 \Leftrightarrow 0 \leq z < \infty \quad (60)$$

The infinite-redshift state is therefore a limiting state in the TDC formulation rather than a finite timelike state.

4.8 Result

Mitra's ECO treatment and TDC use different primary variables to parameterize the same spherical redshift behavior. Mitra uses z, while TDC uses T_o and dR_t. Once the common spherical compactness relation is specified, the mapping is exact:

$$1 + z = 1/T_o = 1/(1 - dR_t) \quad (61)$$

Consequently, the ECO limit $z \to \infty$ corresponds to the TDC limit $dR_t \to 1$ and $T_o \to 0$. This mapping will be used in Section 5 to compare the local gravitational acceleration and the Eddington-balance condition, where the factor (1 + z) is obtained from the radial gradient of the TDC time-rate field.

5. TDC Gravitational Force Gradient and the Local Eddington Limit

The preceding sections established the exact mapping between Mitra's gravitational-redshift parameter and the TDC variables T_o and dR_t after adoption of the common spherical compactness factor. The next comparison concerns the Eddington luminosity of an ultra-compact radiating object. Mitra's ECO treatment contains an enhancement of the locally defined Eddington luminosity by the factor (1 + z). In this section that factor is obtained from the radial gradient of the TDC time-rate differential. Standard radiation-pressure physics is then used to convert the resulting local gravitational acceleration into an Eddington-balance condition.

5.1 Mitra's relativistic local Eddington luminosity

For a spherical relativistic radiation-pressure-supported object, Mitra writes the locally defined Eddington luminosity in the form

$L_{Edd,loc} = (4\pi GMc/\kappa)(1 + z)$ Mitra relativistic local Eddington luminosity.

Here $L_{Edd,loc}$ is the luminosity measured locally at the radiating surface, M is the gravitational mass, G is Newton's gravitational constant, c is the invariant speed of light, κ is the opacity of the radiating material, and z is the gravitational redshift at the surface. The factor (1 + z) distinguishes the relativistic local expression from the Newtonian Eddington luminosity $4\pi GMc/\kappa$.

The comparison below asks whether this enhancement factor follows from the TDC time-rate gradient under the same spherical, quasi-static local-balance assumptions.

5.2 Radial gradient of the TDC time-rate differential

From Sections 2–4, the TDC gravitational time-rate differential for the exterior spherical field may be written

$$dR_t = 1 - \sqrt{(1 - 2GM/(rc^2))} \tag{62}$$

In this section r denotes a general areal radial coordinate at which the field is evaluated; R denotes the radiating surface radius. For the radial derivative used here, M is held fixed over the local differentiation and represents the spherical gravitational mass parameter appropriate to the exterior field at that instant.

Differentiating Equation (62) with respect to r gives

$$d(dR_t)/dr = -GM/(r^2c^2T_o) \tag{63}$$

The negative sign indicates that dR_t decreases outward. Here T_o is the local time-rate factor at radius r, defined by

$$T_o = \sqrt{(1 - 2GM/(rc^2))} \tag{64}$$

Equivalently, the inward magnitude of the radial derivative is

$$-d(dR_t)/dr = GM/(r^2c^2T_o) \tag{65}$$

and the magnitude of the spatial gradient may be written

$$\nabla dR_t = GM/(r^2c^2T_o) \tag{66}$$

5.3 TDC gravitational acceleration

The TDC force-gradient prescription associates the local inward gravitational acceleration with the radial derivative of dR_t:

$$g_{TDC} = -c^2\, d(dR_t)/dr \tag{67}$$

Substituting Equation (65) into Equation (67) gives

$$g_{TDC} = GM/(r^2T_o) \tag{68}$$

At the radiating surface r = R,

$$g_{TDC}(R) = GM/(R^2T_o) \tag{69}$$

Using $1/T_o = 1 + z$ from Section 4,

$$g_{TDC}(R) = (GM/R^2)(1 + z) \tag{70}$$

Thus the factor (1 + z) follows here from differentiating the TDC time-rate field. In the weak-field limit $T_o \to 1$ and $z \to 0$, Equation (70) reduces to GM/R^2.

5.4 Physical regime of the local Eddington balance

The Eddington relation used below is a model condition for the radiating surface, not a generic property of arbitrary relativistic collapse. The calculation assumes: (1) spherical symmetry, so that the local outward radiative flux is distributed over area $4\pi R^2$; (2) a locally quasi-static surface layer, so that gravitational and radiative accelerations can be compared instantaneously; (3) outward, approximately radial radiation interacting with matter through a flux-mean opacity κ; and (4) a regime in which the radiative acceleration can be represented by $\kappa F/c$.

The opacity κ may in general depend on composition, temperature, density, and photon spectrum. If electron scattering dominates in fully ionized material it may be approximated by the corresponding scattering opacity; the derivation itself does not require κ to be numerically constant except when a constant value is adopted in the later dynamical model.

Optical depth also limits the interpretation. In an optically thick layer, the flux entering the force law is the local transported radiative flux and may be diffusion-limited; in an optically thin scattering layer, $\kappa F/c$ represents the local momentum transfer per unit mass. Strong photon trapping, substantial advective transport, anisotropic escape, convection, magnetic stresses, or nonspherical outflow would require a fuller radiation-hydrodynamic treatment. Those effects are outside the local spherical balance condition tested here.

5.5 Radiation-pressure acceleration

If L_{loc} is the luminosity measured locally at radius R, spherical symmetry gives the local radiative flux

$$F_{rad} = L_{loc}/(4\pi R^2) \tag{71}$$

where F_{rad} is energy flux, not force. For flux-mean opacity κ, the corresponding outward radiative acceleration is

$$a_{rad} = \kappa F_{rad}/c \tag{72}$$

Substitution of Equation (71) gives

$$a_{rad} = \kappa L_{loc}/(4\pi R^2 c) \tag{73}$$

5.6 Local Eddington balance in TDC

Within the physical regime specified in Section 5.4, the local Eddington condition is the instantaneous equality of outward radiative acceleration and inward TDC gravitational acceleration:

$$a_{rad} = g_{TDC} \tag{74}$$

Using Equations (69) and (73),

$$\kappa L_{loc}/(4\pi R^2 c) = GM/(R^2 T_o) \tag{75}$$

The factor R^2 cancels, giving

$$L_{Edd,loc} = 4\pi GMc/(\kappa T_o) \tag{76}$$

Using $T_o = 1 - dR_t$,

$$L_{Edd,loc} = 4\pi GMc/[\kappa(1 - dR_t)] \quad (77)$$

and using $1/T_o = 1 + z$,

$$L_{Edd,loc} = (4\pi GMc/\kappa)(1 + z) \quad (78)$$

5.7 Direct Mitra–TDC comparison

Mitra's ECO expression and Equation (78) are algebraically identical. The distinction lies in the route to the enhancement factor. In the present TDC model, $1/T_o$ is generated by the spatial derivative of the TDC time-rate differential, after which the standard local radiation-force relation $a_{rad} = \kappa F_{rad}/c$ is imposed as the balance condition.

This correspondence should therefore be read as a result within the stated spherical quasi-static radiative model, not as a claim that every collapsing configuration must remain at an Eddington balance.

5.8 Behavior near the limiting compactness

From Equation (77), as dR_t approaches unity from below, the local Eddington luminosity increases for finite positive M and κ at a given stage of the evolution:

$$dR_t \to 1^- \Rightarrow L_{Edd,loc} \to \infty \quad (79)$$

This is a local requirement. It does not imply that a distant observer measures an indefinitely increasing luminosity. The photon-energy redshift and arrival-rate time dilation derived in Section 4 suppress the luminosity received at infinity; that transformation is treated in Section 6.

5.8.1 Consistency conditions at high gravitational redshift

The increase of the local Eddington luminosity as T_o decreases is an instantaneous requirement of the assumed balance, not evidence that a collapsing surface can maintain that balance arbitrarily close to $T_o = 0$. At each stage, the radiation field must supply the local flux $L_{edd,loc}/(4\pi R^2)$, and its momentum transfer must remain describable by a flux-mean opacity κ. The present reduced system does not solve for the temperature, density, optical depth, composition, or radiation spectrum that would determine whether this flux is physically sustainable.

In particular, a constant κ is a baseline closure, not a demonstrated high-redshift material property. Ionization, frequency-dependent scattering or absorption, pair production, and changing composition can alter the effective opacity. If κ varies with radius or time, both the local Eddington condition and the constant-A evolution of Sections 8–9 must be recalculated. The assumed spherical flux also requires angularly averaged transport to remain approximately radial; magnetic collimation, rotation, jets, and anisotropic leakage would invalidate a single isotropic Eddington luminosity.

Quasi-static balance additionally requires that surface acceleration, contraction, and changes in the mass and radiation field be slow compared with the local hydrodynamic and radiative adjustment times. The distant-observer light-crossing condition in Section 7.3 is necessary for the adopted instantaneous exterior approximation but does not by itself establish local hydrostatic or radiative equilibrium. As T_o becomes small, strong gradients, photon trapping, diffusion delays, and radiation advection can prevent the locally produced luminosity from escaping according to the simple $L_\infty = T_o^2 L_{loc}$ mapping. A self-consistent calculation would need the interior equation of state, radiative transfer, optical-depth profile, and surface matching throughout the evolution.

Finally, the divergence $L_{edd,loc} \propto M/(\kappa T_o)$ applies at fixed instantaneous M and κ. Along the coupled solution M also decreases, so the absolute local luminosity cannot be inferred from T_o alone. The calculations in this paper establish the conditional Eddington-regulated branch and its asymptotic behavior; they do not demonstrate that a physical material configuration remains spherical, quasi-static, or Eddington-regulated at arbitrarily high redshift. Failure of any of these conditions would require a different dynamical closure and could change the inferred limiting evolution.

5.9 Scope and result

The local factor $1/T_o = 1 + z$ follows from the adopted TDC time-rate gradient; the Eddington balance then uses the standard radiation-force law under the conditions of Section 5.4.

The resulting local luminosity agrees with Mitra's ECO expression. Section 6 applies the observer transformations to obtain the luminosity at infinity.

6. Luminosity at Infinity and the ECO Redshift Suppression

Section 5 showed that, under the stated spherical quasi-static Eddington-balance conditions, the TDC time-rate gradient produces the same local relativistic Eddington luminosity used in Mitra's ECO treatment. The luminosity measured by the distant observer is not equal to the luminosity measured locally at the emitting surface. Each photon is gravitationally redshifted, and the photon arrival rate is reduced by gravitational time dilation. This section combines the two transformations already established in Section 4 and compares the result with Mitra's distant-luminosity relation.

6.1 Mitra's luminosity observed at infinity

Mitra states that the luminosity observed by a distant astronomer is lower than the locally defined luminosity by a factor $(1 + z)^2$ because of the joint effects of gravitational redshift and gravitational time dilation. His relation may be written

$L_\infty = L_{loc}/(1 + z)^2$ Mitra [2006, Eq. (42)], distant-observer luminosity relation.

Here L_{loc} is the luminosity measured locally at the emitting surface, L_∞ is the luminosity received by an observer at infinity, and z is the surface gravitational redshift. Applied to the locally defined Eddington luminosity, this relation gives

$L_{Edd,\infty} = L_{Edd,loc}/(1 + z)^2$ Mitra ECO Eddington luminosity observed at infinity.

Section 5 established, within the specified local-balance model, $L_{Edd,loc} = (4\pi GMc/\kappa)(1 + z)$. Substitution gives

$L_{Edd,\infty} = 4\pi GMc/[\kappa(1 + z)]$ Mitra ECO distant Eddington luminosity.

6.2 TDC photon-energy redshift

Section 4 established the mapping between the local surface time-rate factor and gravitational redshift:

$$T_o = 1/(1 + z) \tag{80}$$

For photon frequency, with ν_{loc} measured locally and ν_∞ measured by the distant observer,

$$\nu_\infty = T_o \nu_{loc} \tag{81}$$

Since photon energy is E = hν, the same factor applies to the energy assigned to each photon by the two observers:

$$E_\infty = T_o E_{loc} \tag{82}$$

Thus each photon received at infinity carries the fraction $T_o = 1/(1 + z)$ of the energy assigned to it by the local emitting observer.

6.3 TDC photon-arrival-rate dilation

The second factor follows from the time-rate relation already established in Section 4. If dτ is the local proper-time interval and dt_∞ is the corresponding distant-observer interval,

$$d\tau = T_o \, dt_\infty \tag{83}$$

so that

$$d\tau/dt_\infty = T_o \tag{84}$$

If dN photons are emitted during dτ, the local number rate is dN/dτ. The corresponding distant-observer rate is therefore

$$dN/dt_\infty = T_o(dN/d\tau) \tag{85}$$

The photon-arrival rate is consequently reduced by the same factor T_o that reduces the energy assigned to each photon.

6.4 TDC luminosity transformation

Luminosity is energy per unit observer time. Combining Equations (82) and (85) gives

$$L_\infty = T_o^2 L_{loc} \tag{86}$$

Using $T_o = 1 - dR_t$,

$$L_\infty = (1 - dR_t)^2 L_{loc} \tag{87}$$

and using $1 + z = 1/T_o$,

$$L_\infty = L_{loc}/(1 + z)^2 \tag{88}$$

Equation (88) is algebraically identical to Mitra's distant-observer luminosity relation. In the TDC parameterization, the two factors of T_o are displayed separately: one arises from the photon-energy shift and the other from the relation between local proper time and distant-observer time.

6.5 Compactness form of the luminosity suppression

From the common spherical compactness relation, $T_o^2 = 1 - 2GM/(Rc^2)$. Equation (86) may therefore be written directly as

$$L_\infty = [1 - 2GM/(Rc^2)]L_{loc} \tag{89}$$

This form makes the compactness dependence explicit. As $2GM/(Rc^2)$ approaches unity from below, the luminosity assigned by the distant observer becomes an increasingly small fraction of the local luminosity.

6.6 Eddington luminosity at infinity

Section 5 obtained the local TDC Eddington-balance luminosity

$$L_{Edd,loc} = 4\pi GMc/(\kappa T_o) \quad (90)$$

Applying Equation (86),

$$L_{Edd,\infty} = T_o{}^2 L_{Edd,loc} \quad (91)$$

and hence

$$L_{Edd,\infty} = (4\pi GMc/\kappa)T_o \quad (92)$$

Equivalently, Equation (92) gives $L_{Edd,\infty} = (4\pi GMc/\kappa)(1 - dR_t)$. In terms of gravitational redshift,

$$L_{Edd,\infty} = 4\pi GMc/[\kappa(1 + z)] \quad (93)$$

Equation (93) is the same distant Eddington luminosity used in Mitra's ECO treatment. Its derivation here combines the TDC local force-gradient result of Section 5 with the observer transformations established in Section 4.

6.7 Opposite local and distant limiting behavior

The local and distant Eddington luminosities have opposite redshift dependence at a fixed instantaneous M and κ. From Sections 5 and 6,

$$L_{Edd,loc} \propto 1/T_o \propto (1 + z) \quad (94)$$

$$L_{Edd,\infty} \propto T_o \propto 1/(1 + z) \quad (95)$$

Thus, for fixed positive M and κ at a given stage of the sequence, $T_o \to 0$ causes the local Eddington requirement to increase while the luminosity measured at infinity decreases. These are instantaneous scaling relations; in the coupled collapse problem M and R also evolve.

6.8 Energy accounting and interpretation

The relation $L_\infty = T_o{}^2 L_{loc}$ is a relation between luminosities assigned by different observers; it should not be interpreted as local destruction of radiation energy. The local emitter measures its own photon energies, proper-time intervals, and luminosity locally, while the distant observer assigns lower photon energies and a longer time interval according to the transformations above.

For the present comparison, no additional ECO dynamical assumption is required to obtain the factor $(1 + z)^{-2}$ once the common spherical redshift relation and the TDC observer mapping $T_o = 1/(1 + z)$ have been specified. The separate question of how the outgoing luminosity changes the object's gravitational mass is deferred to Section 7, where the mass definition and mass-energy balance must be stated explicitly.

6.9 Result

The TDC expression $L_\infty = T_o{}^2 L_{loc}$ is equivalent to Mitra's $L_\infty = L_{loc}/(1 + z)^2$. Applied to the Eddington balance, it gives $L_{Edd,\infty} = 4\pi GMc/[\kappa(1 + z)]$, used in the mass-loss calculation of Section 7.

7. Mass-Energy Depletion and the Eternally Collapsing Timescale

Sections 5 and 6 established the local and distant Eddington luminosities used in the ECO comparison. The next step is to relate the luminosity measured at infinity to the changing

gravitational mass of the radiating object. Because that identification is essential to the depletion timescale, the mass convention and exterior radiating geometry are stated explicitly before the calculation.

7.1 Mitra's Einstein–Eddington depletion timescale

Mitra defines the observed depletion time by comparing the mass-energy Mc^2 with the Eddington luminosity measured at infinity. His result may be written

$t = [\kappa c/(4\pi G)](1 + z)$ Mitra [2006, Eq. (43)], observed mass-energy depletion timescale.

Mitra notes that the coefficient $\kappa c/(4\pi G)$ is independent of M. The central limiting result is $t \to \infty$ as $z \to \infty$, which supplies the basis for the designation “eternally collapsing object.”

7.2 Gravitational-mass convention and radiating exterior

For the radiating spherical model used here, M is defined operationally as the mass parameter of the exterior outgoing Vaidya geometry. At the stellar surface this mass parameter is matched to the spherical Misner–Sharp mass of the interior; at large radius its decreasing value is the gravitational mass inferred by the distant observer from the outgoing radiative flux. Thus M in the depletion equations is not a local rest-mass integral and is not assumed constant during radiation [9,10].

The corresponding conventional exterior spacetime for spherical outgoing null radiation may be written in retarded time u as

$$ds^2 = -(1 - 2GM/(Rc^2))c^2du^2 - 2c\,du\,dR + R^2d\Omega^2 \tag{96}$$

with M = M(u). In the no-radiation limit, M is constant and Equation (96) reduces to the Schwarzschild exterior in outgoing null coordinates. The surface is taken to be a timelike matching hypersurface Σ. Standard radiating-star matching requires continuity of the induced metric and extrinsic curvature; in spherical symmetry the exterior Vaidya mass parameter at Σ equals the interior Misner–Sharp mass evaluated at the surface [11,12].

TDC 10 does not attempt to construct a new interior radiating-star solution or new junction conditions. The Vaidya exterior and standard spherical matching are adopted here to state precisely the conventional mass and radiation bookkeeping used when the TDC surface relations are allowed to evolve.

7.3 Quasi-static use of the surface compactness relation

The surface relation $T_o^2 = 1 - 2GM/(Rc^2)$ is used during radiation as an instantaneous, quasi-static compactness relation rather than as a claim that the entire exterior is exactly Schwarzschild while M varies. The approximation requires M and R to change negligibly over a surface light-crossing time. A convenient statement of this condition is

$$|dR/dt_\infty| \ll c, \quad |dM/dt_\infty| \ll Mc/R \tag{97}$$

Under these conditions the instantaneous $M(t_\infty)$ and $R(t_\infty)$ may be inserted into the spherical surface compactness factor while the outgoing radiation is accounted for by the Vaidya mass loss. This is the approximation used in the depletion calculation below.

7.4 Mass-energy balance at infinity

Let L_∞ denote the outward luminosity measured by the distant observer and t_∞ the corresponding distant-observer time. With M defined as above, conservation of energy for the outgoing radiative flux gives

$$L_\infty = -c^2\, dM/dt_\infty \tag{98}$$

The minus sign indicates that positive outward luminosity corresponds to decreasing gravitational mass. Equation (98) is therefore the mass-loss law for the exterior gravitational mass used in this model; it is not an identification of local material rest mass with distant luminosity.

7.5 TDC Eddington-limited mass loss

Section 6 gives the distant Eddington luminosity

$$L_{Edd,\infty} = (4\pi GMc/\kappa)T_o \tag{99}$$

For Eddington-limited radiation, substitution of Equation (99) into Equation (98) gives

$$-c^2\, dM/dt_\infty = (4\pi GMc/\kappa)T_o \tag{100}$$

and therefore

$$dM/dt_\infty = -(4\pi G/\kappa c)T_o\, M \tag{101}$$

Dividing by M gives the fractional gravitational-mass loss rate

$$(1/M)dM/dt_\infty = -(4\pi G/\kappa c)T_o \tag{102}$$

7.6 Instantaneous depletion timescale

Define the positive instantaneous gravitational-mass depletion timescale by

$$\tau_M \equiv -M/(dM/dt_\infty) \tag{103}$$

Substitution of Equation (101) yields

$$\tau_M = \kappa c/(4\pi GT_o) \tag{104}$$

Using $T_o = 1 - dR_t$, Equation (104) is equivalently $\tau_M = \kappa c/[4\pi G(1 - dR_t)]$. Using $1 + z = 1/T_o$, this becomes

$$\tau_M = [\kappa c/(4\pi G)](1 + z) \tag{105}$$

Equation (105) is algebraically identical to Mitra's Einstein–Eddington depletion timescale. Here it is explicitly an instantaneous timescale for the exterior gravitational mass under the Eddington-limited, quasi-static spherical model.

7.7 Limiting behavior and interpretation

As the compactness limit is approached, $T_o \to 0$ and $z \to \infty$, so

$$\tau_M \rightarrow \infty \tag{106}$$

At every finite timelike state T_o remains positive and the instantaneous depletion time remains finite. The divergence occurs only in the limiting state. The cancellation of M in Equation (105) follows because both the available gravitational mass-energy scale Mc^2 and the Eddington luminosity are proportional to the instantaneous M.

This characteristic timescale should not be read as the exact elapsed lifetime of an evolving object unless the redshift factor is held fixed. When M, R, and therefore T_o evolve together, the actual history follows from integrating Equation (101) simultaneously with the radius evolution. That coupled problem is treated later in the paper.

7.7.1 Exterior energy balance, moving surface, and elapsed time

The mass-loss relation in Equation (98) has two distinct levels of validity. In an outgoing Vaidya exterior, with mass parameter M defined in terms of retarded null time (denoted u in Equation (96)), the outgoing luminosity measured at future null infinity satisfies $L_\infty = -c^2\, dM/du$ as an exterior energy-flux identity. This retarded-time coordinate u is unrelated to the local inward contraction speed u defined in Equation (114). Identifying the retarded-time derivative with dM/dt_∞ in Equation (98) requires the adopted distant-observer time convention and a corresponding normalization of the asymptotic retarded time; applying the instantaneous static-surface redshift to the moving emitting surface additionally invokes the quasi-static approximation of Section 7.3.

The exterior Vaidya mass parameter already accounts for the net gravitational energy carried away by outgoing radiation in the specified spherical null-radiation model. No separate exterior-field energy reservoir is introduced in that model. This does not mean that the interior energy partition is known: changes in matter internal energy, kinetic energy, binding energy, and radiation temporarily stored or trapped between the emitting layers and infinity are not separately computed. If such storage, scattering, or delayed escape is significant, the instantaneous identification of surface emission with luminosity at infinity needs a radiation-transport calculation, and the simple luminosity transformation of Section 6 may require correction.

The coupling assumed here is explicit but conditional. The local Eddington prescription fixes L_{loc} at the instantaneous M, R, and opacity κ; the quasi-static redshift prescription sets $L_\infty = T_o^2\, L_{loc}$; the exterior flux balance fixes the resulting loss of M; and the independently prescribed contraction speed fixes the change in R through Equation (115). The algebraic compactness relation then updates T_o and ε. These prescriptions close the reduced surface system, but they are not a derived interior radiation-hydrodynamic conservation law. The conditions in Sections 5.4, 7.3, and 8.5 must remain valid along any physical trajectory.

The depletion time $\tau M = M/|dM/dt_\infty|$ in Equations (103)–(105) is an instantaneous e-folding scale, not the elapsed time to reach a specified radius or compactness. For the constant-u baseline of Sections 8–9, $dx/ds = -\varepsilon$ and $s = At_\infty$. Thus the elapsed distant-observer time between x_0 and a smaller positive x_f is $\Delta t_\infty = (1/A) \int_{x_f}^{x_0} dx/\varepsilon(x)$, evaluated along the coupled solution. The asymptotic result $\varepsilon(x) \sim x^2$, when applicable, makes this integral diverge as x_f tends to zero, whereas any finite interval with $\varepsilon > 0$ has a finite elapsed time. This divergence is a property of the prescribed reduced evolution and does not independently establish the global causal absence of a horizon.

7.8 Result

Under the spherical, quasi-static Eddington-limited assumptions, the instantaneous TDC depletion timescale is $\tau M = [\kappa c/(4\pi G)](1 + z)$, matching the ECO relation. Section 8 evolves M and R simultaneously.

8. Coupled Evolution of Mass, Radius, and Time Rate

The preceding sections compared instantaneous ECO relations with corresponding TDC relations. A dynamical model must allow the gravitational mass M, areal radius R, surface time-rate factor T_o, and redshift z to evolve together. As radiation carries energy to infinity, M decreases; as contraction continues, R decreases; and both changes alter the compactness and therefore T_o. This section develops that coupled evolution under the spherical, quasi-static, Eddington-limited assumptions stated in Sections 5–7.

The exterior radiating geometry and mass convention are those specified in Section 7: M is the outgoing Vaidya mass parameter, matched at the timelike surface to the interior Misner–Sharp mass, while the spherical compactness factor is used instantaneously under the quasi-static conditions of Equation (97). The equations below therefore do not treat a time-varying object as an exactly static Schwarzschild exterior.

8.1 Compactness departure variable

Define the dimensionless departure from the limiting spherical compactness by

$$\varepsilon = 1 - 2GM/(Rc^2) \tag{107}$$

For a finite timelike TDC state, $0 < \varepsilon \leq 1$. From the TDC surface time-rate relation,

$$\varepsilon = T_o{}^2 \tag{108}$$

Solving Equation (107) for M gives

$$M = (Rc^2/2G)(1 - \varepsilon) \tag{109}$$

Thus M, R, and ε are linked and cannot be prescribed independently.

8.2 General differential relation between mass and radius

Allow M, R, and ε to depend on distant-observer time t_∞. Logarithmic differentiation of $1 - \varepsilon = 2GM/(Rc^2)$ gives

$$d\varepsilon/dt_\infty = (1 - \varepsilon)[(1/R)dR/dt_\infty - (1/M)dM/dt_\infty] \tag{110}$$

Equation (110) is kinematic: radial contraction drives ε downward, while loss of gravitational mass at fixed radius drives ε upward.

8.3 Radiative mass-loss law

Section 7 gives the Eddington-limited gravitational-mass loss law

$$dM/dt_\infty = -AMT_o \tag{111}$$

where

$$A = 4\pi G/(\kappa c) \tag{112}$$

and therefore, using $T_o = \sqrt{\varepsilon}$,

$$(1/M)dM/dt_\infty = -A\sqrt{\varepsilon} \tag{113}$$

The constant-A form assumes the prescribed opacity κ used in the baseline model. A variable opacity would make A time dependent and is outside the present comparison.

8.4 TDC radial contraction law

Let u denote the positive magnitude of the inward contraction speed measured with local proper radial distance ℓ and local proper time τ:

$$u = -d\ell/d\tau \tag{114}$$

Section 2 derived the reciprocal radial scaling $d\ell = dR/T_o$, while $d\tau = T_o\, dt_\infty$. Substitution into Equation (114) gives

$$dR/dt_\infty = -uT_o^{\,2} = -u\varepsilon \tag{115}$$

Equation (115) is the radial contraction law used in the coupled model. It follows from the explicitly stated TDC reciprocal radial scaling and the definition of the local contraction parameter u; it is not a general relativistic collapse law.

8.5 Physical Status and Limitations of the Contraction Prescription

The radial relation in Equation (115) follows from the adopted reciprocal temporal–radial scaling and the definition of the local inward contraction parameter u. It is a conversion between locally specified contraction and the distant-observer evolution of the areal radius, not an independent equation of motion for the collapsing material. In particular, neither Equation (115) nor the spherical compactness relation determines u from a pressure gradient, equation of state, or interior gravitational dynamics. The constant-u choice employed in the baseline system of Section 8.8 is therefore a prescribed closure used to examine the consequences of the coupled mass–radius equations. It should not be interpreted as a demonstrated dynamical outcome of collapse.

The mass-loss law likewise assumes that the radiating surface remains near the local Eddington balance described in Section 5.4, with an effective opacity κ specified for the baseline calculation. This condition may be physically relevant to a radiation-supported surface, but the present treatment does not solve radiation transport or show that a collapsing configuration necessarily reaches or maintains that balance. Changes in opacity, optical depth, photon trapping, advection, convection, anisotropic emission, or magnetic stresses could alter the luminosity and hence the compactness evolution. The attracting trajectory found in Section 9 is consequently a result for this radiative closure, not a prediction for arbitrary collapse.

The quasi-static surface approximation stated in Section 7.3 introduces a further consistency requirement. Its use is justified only over intervals for which the fractional changes of mass and radius during the relevant surface light-crossing time remain small. In the present model, this requirement must be checked along the computed trajectories rather than inferred solely from the numerical convergence of the differential equations. In particular, behavior very close to the compactness limit may demand a time-dependent treatment of the exterior geometry and surface matching beyond the instantaneous spherical factors used here. The current integrations establish

properties of the reduced system but do not by themselves verify the quasi-static approximation at every stage.

Finally, the stability analysis in Section 9 concerns attraction of solutions of the prescribed two-variable evolution system. It does not constitute a perturbative stability analysis of a self-gravitating radiating fluid, nor does it prove that trapped surfaces or an event horizon are excluded in a fully dynamical spacetime. Establishing those stronger conclusions would require an interior matter model, coupled radiation hydrodynamics, appropriate matching conditions, and a causal analysis of the resulting geometry. These qualifications delimit the physical claims of the present TDC–ECO comparison while leaving its conditional mathematical predictions available for testing.

The quasi-static approximation is an additional condition on the applicability of the reduced evolution model. Although the numerical integrations establish the behavior of the coupled equations under this approximation, they do not independently demonstrate that the quasi-static consistency conditions remain satisfied throughout every trajectory, particularly as $\varepsilon \to 0$). The resulting asymptotic behavior should therefore be understood as conditional on the continued validity of this approximation.

8.5.1 Equation count, conservation input, and dynamical closure

The reduced surface model contains three time-dependent quantities, $M(t_\infty)$, $R(t_\infty)$, and $\varepsilon(t_\infty)$, constrained algebraically by Equation (109). Thus only two independent evolution functions remain. The adopted outgoing-radiation balance supplies one differential equation: Equation (113) specifies the gravitational-mass loss rate when the luminosity at infinity is set equal to the Eddington-limited value. Equation (115) supplies the second differential relation only after the locally defined inward contraction speed u is prescribed. Equation (110) then determines ε consistently from M and R; Equation (117) is not an additional independent conservation law.

The independent physical inputs are therefore (i) the spherical surface compactness and reciprocal radial scaling, (ii) the outgoing radiative mass-energy balance with the assumed Eddington luminosity and opacity, and (iii) the contraction closure $u(t_\infty,M,R,\varepsilon)$, taken as constant in the baseline integrations. Initial values for two independent variables complete the reduced initial-value problem. The algebraic compactness relation and its differentiated form must not be counted as independent dynamical field equations.

For the outgoing Vaidya exterior, the decrease of its mass parameter is associated with positive outward null energy flux, as stated in Section 7. This supplies exterior radiative energy bookkeeping under the adopted mass definition. It does not by itself establish local conservation throughout an unspecified interior: a complete demonstration would require an interior stress-energy tensor, the equations governing its fluid and radiation components, and junction conditions showing that the surface flux matches the exterior radiation. The current model does not solve that system.

In particular, u is not obtained from the radial component of an interior momentum-conservation equation. A physical closure would require, at minimum, an equation of state and radial force balance or acceleration equation incorporating pressure gradients, radiation momentum exchange, and any relevant magnetic stresses. Consequently the constant-u and power-law-u cases should be interpreted as conditional dynamical experiments, not a derivation of the material contraction speed from first principles.

The mass-loss relation is exact as exterior flux bookkeeping when formulated with the appropriate Vaidya retarded time and mass convention. Its use together with the instantaneous static-surface redshift, the local

Eddington relation, and the distant-observer time t_∞ is quasi-static and requires the conditions of Section 7.3. In a fully dynamical treatment, retarded-time conversion, surface motion, radiation transport, and interior-to-exterior matching may introduce corrections. The numerical integrations test the reduced closure but cannot alone establish those corrections are negligible.

8.6 Coupled compactness evolution

Substitution of Equations (113) and (115) into Equation (110) gives

$$d\varepsilon/dt_\infty = (1 - \varepsilon)\varepsilon[A/\sqrt{\varepsilon} - u/R] \tag{116}$$

Equivalently,

$$d\varepsilon/dt_\infty = (1 - \varepsilon)[A\sqrt{\varepsilon} - (u/R)\varepsilon] \tag{117}$$

Equations (115) and (117), together with Equation (109), form the coupled system once u is specified. The two terms in Equation (117) have opposite effects: contraction increases compactness and drives ε downward, whereas radiative mass loss reduces compactness and drives ε upward.

The coupled compactness equation also provides a direct test of whether the evolving configuration can reach the limiting compactness at finite radius. In the constant-opacity, constant-contraction-parameter baseline developed below, the dimensionless equations imply that the compactness departure increases whenever $0 < \varepsilon < x^2$. Thus, for any finite positive radius variable x, sufficiently small positive values of ε experience a restoring tendency away from zero. This establishes a barrier against reaching $\varepsilon = 0$ at finite positive x within the specified dynamical model. The stronger question of whether the evolution approaches $\varepsilon = 0$ only asymptotically as $x \to 0$ is examined analytically and numerically in Section 9. These results concern the evolution of the modeled material surface and do not, by themselves, establish the global absence of an event horizon.

8.7 Instantaneous balance and the ECO-like regime

For $0 < \varepsilon < 1$, the instantaneous balance $d\varepsilon/dt_\infty = 0$ occurs when

$$A\sqrt{\varepsilon} = (u/R)\varepsilon \tag{118}$$

so that

$$\sqrt{\varepsilon} = AR/u \tag{119}$$

or

$$\varepsilon = (AR/u)^2 \tag{120}$$

Since $T_o = \sqrt{\varepsilon}$ and $1 + z = 1/T_o$, the same balance may be written

$$T_o = AR/u, \quad 1 + z = u/(AR) \tag{121}$$

This relation is not imposed as an ECO condition. It is the instantaneous point at which contraction and radiative mass loss have equal and opposite effects on compactness.

8.8 Limiting mass-radius behavior

On the balance relation, Equation (109) becomes

$$M = (Rc^2/2G)[1 - (AR/u)^2] \tag{122}$$

For finite positive u and AR/u ≪ 1,

$$M \approx Rc^2/(2G) \tag{123}$$

Thus the near-Schwarzschild mass-radius behavior appearing in Mitra's extreme-redshift ECO discussion arises here as the limiting form of the coupled TDC balance relation rather than being inserted as an initial identity.

8.9 Baseline dimensionless system for constant u

For the baseline stability calculation, take u to be finite and approximately constant over the interval examined and define

$$x = AR/u, \quad s = At_\infty \tag{124}$$

Equations (115) and (117) then become

$$dx/ds = -\varepsilon \tag{125}$$

$$d\varepsilon/ds = (1 - \varepsilon)(\sqrt{\varepsilon} - \varepsilon/x) \tag{126}$$

The instantaneous balance relation is simply

$$\varepsilon = x^2 \tag{127}$$

Equations (125)–(127) are the dimensionless system tested numerically in Section 9. The constant-u assumption is a baseline closure prescription, not a claim that the local contraction speed must be exactly constant throughout physical collapse.

8.9.1 Notation, physical dimensions, and SI normalization

The notation in the coupled system is fixed as follows. M is the exterior gravitational mass (kg); R is the surface areal radius (m); t_∞ is distant-observer time (s); τ is local proper time (s); u is the prescribed positive local inward contraction speed (m s^{-1}); κ is opacity (m^2 kg^{-1}); and G and c retain SI units m^3 kg^{-1} s^{-2} and m s^{-1}. The time-rate factor T_o, compactness departure $\varepsilon = T_o^2$, and gravitational redshift z are dimensionless. The exterior retarded-time coordinate u appearing in the Vaidya discussion is a distinct quantity from the contraction speed u; no identification between them is intended.

In the constant-opacity baseline, $A = 4\pi G/(\kappa c)$ has units s^{-1}: $[G]/([\kappa][c]) = (m^3\ kg^{-1}\ s^{-2})/[(m^2\ kg^{-1})(m\ s^{-1})] = s^{-1}$. Consequently $x = AR/u$ and $s = At_\infty$ are both dimensionless. Differentiation with respect to s therefore introduces a factor 1/A relative to differentiation with respect to t_∞; x is a normalized areal radius, not a physical distance. The dimensionless exponent q in the variable-u sensitivity family is likewise unitless.

The SI compactness relation $\varepsilon = 1 - 2GM/(Rc^2)$ is dimensionless because $[GM] = m^3\ s^{-2}$ and $[Rc^2] = m^3\ s^{-2}$. The luminosity $4\pi GMcT_o/\kappa$ has units kg m^2 s^{-3} (watts), while L_∞/c^2 has units kg s^{-1}, consistent with the gravitational-mass loss law. The depletion scale $\kappa c/(4\pi GT_o)$ has units seconds. These dimensional checks

apply to the SI expressions; the geometrized Mitra relations quoted with G = c = 1 must have the appropriate G and c restored before numerical comparison.

Throughout the numerical analysis, the logarithmic independent variable $\tau = -\ln x$ in Section 9.5.1 is dimensionless and is not the local proper time τ used elsewhere in the manuscript. It is a numerical reparameterization only. In reproducing that calculation, use the specified independent variable and avoid interpreting its derivative as a proper-time derivative. This notation overlap does not affect the differential equation but should be observed when translating between the numerical and physical systems.

8.10 Sensitivity to a variable contraction parameter u

The sensitivity of the constant-u closure can be tested without changing the physical coupled equations (115) and (117). As a specified sensitivity family, let the local contraction parameter vary with radius as

$$u(R) = u_0(R/R_0)^q \tag{128}$$

where $u_0 > 0$ is the contraction parameter at reference radius R_0 and q is a dimensionless logarithmic slope. The constant-u baseline is q = 0.

Substitution into the instantaneous balance condition, Equation (120), gives

$$\varepsilon = [AR_0/u_0]^2(R/R_0)^{(2-2q)} \tag{129}$$

Therefore the approach $\varepsilon \to 0$ as $R \to 0$ is not restricted mathematically to q = 0. For this power-law family it persists whenever q < 1; q = 1 gives a constant balance value of ε, while q > 1 reverses the small-R trend. The asymptotic exponent is consequently sensitive to the contraction prescription even though the competition represented by Equation (117) remains unchanged.

Section 9 will retain q = 0 for the primary phase-space comparison with the original numerical integrations and will separately test representative nonzero q values as a sensitivity check. This separates the demonstrated constant-u attractor from conclusions that depend on how u evolves.

8.11 Asymptotic scaling in the baseline model

For q = 0, the candidate balance $\varepsilon = x^2$ inserted into Equation (125) gives

$$dx/ds = -x^2 \tag{130}$$

which integrates to

$$1/x = s + K \tag{131}$$

where K is an integration constant. Hence at sufficiently large s,

$$x \propto s^{-1}, \quad \varepsilon \propto s^{-2} \tag{132}$$

Because $x = AR/u$ and $s = At_\infty$ for constant A and u, the candidate baseline scaling is $R \propto t_\infty^{-1}$, with $M \propto R$ in the extreme compactness limit. These remain candidate asymptotic relations until the stability and numerical tests of Section 9 are applied.

8.12 Scope and result

The coupled equations describe a specified spherical, quasi-static, Eddington-limited radiative model with prescribed opacity and local contraction parameter u; they are not general collapse equations.

Within the constant-u baseline, the instantaneous balance is $\varepsilon = x^2$ and the candidate limiting behavior is $T_o \to 0$, $z \to \infty$, and $M \approx Rc^2/(2G)$. The variable-u family in Equation (128) shows explicitly which part of that conclusion is robust and which part depends on the closure prescription: for $u \propto R^q$ the balance still approaches $\varepsilon \to 0$ for $q < 1$, but with the modified exponent $2(1 - q)$. Section 9 now tests whether trajectories actually converge toward the baseline relation and examines the specified variable-u sensitivity.

9. Stability and Numerical Evolution of the TDC-ECO Limit

Section 8 derived the coupled dimensionless system for the radius variable x and compactness-departure variable ε and identified $\varepsilon = x^2$ as the candidate balance relation for the constant-u baseline. A balance relation alone does not establish dynamical attraction. This section therefore examines the local restoring tendency, integrates trajectories beginning on both sides of the candidate curve, and then considers the variable-u sensitivity introduced in Section 8.10.

9.1 Dimensionless evolution system

For finite constant local contraction parameter u, Section 8 defined $x \equiv AR/u$ and $s \equiv At_\infty$. The evolution equations are

$$dx/ds = -\varepsilon \tag{133}$$

$$d\varepsilon/ds = (1 - \varepsilon)(\sqrt{\varepsilon} - \varepsilon/x) \tag{134}$$

The candidate balance relation is

$$\varepsilon = x^2 \tag{135}$$

Here x, ε, and s are dimensionless. During contraction x decreases because $\varepsilon > 0$.

9.2 Analytical Stability of the Asymptotic Trajectory

The instantaneous balance curve $\varepsilon = x^2$ identified in Section 9.1 is not itself an exact solution trajectory, because x continues to evolve along it. To investigate attraction toward this curve, introduce the dimensionless ratio

$$y = \frac{\sqrt{\varepsilon}}{x}. \tag{136}$$

Using Equations (133) and (134), with $dx/ds = -\varepsilon$ and $d\varepsilon/ds = (1 - \varepsilon)\left(\sqrt{\varepsilon} - \varepsilon/x\right)$, differentiation yields

$$\frac{dy}{ds} = \frac{(1-\varepsilon)(1-y)}{2x} + xy^3. \tag{137}$$

For $0 < y < 1$ and $0 < \varepsilon < 1$, both terms on the right are positive, so y increases. For $y > 1$, the first term is negative and acts as a restoring contribution, while the second term remains positive.

Consequently, $y = 1$ is not an exact stationary curve at finite x; the relevant claim is asymptotic attraction as $x \to 0^+$.

To determine the leading correction, consider the following formal asymptotic expansion: $y = 1 + ax^2 + O(x^4)$ and use $\varepsilon = x^2y^2$ and $dx/ds = -x^2y^2$. At leading order, the right side of Equation (137) is $(1 - a/2)x + O(x^3)$, whereas the derivative along the proposed expansion is $O(x^3)$. Cancellation of the order-x term requires $a = 2$. Thus the formal asymptotic expansion is

$$y = 1 + 2x^2 + O(x^4), \tag{138}$$

Here, $O(x^4)$ denotes terms bounded in magnitude by a constant multiple of x^4 as $x \to 0$, representing the higher-order corrections omitted from the asymptotic expansion. Hence,

$$\frac{\varepsilon}{x^2} = 1 + 4x^2 + O(x^4). \tag{139}$$

This calculation gives the leading correction for a trajectory that enters the asymptotic regime; it is not by itself a global stability theorem for every admissible initial condition. The numerical trajectories and their sensitivity to the contraction prescription should therefore be retained as complementary tests. Furthermore, positivity of the surface compactness departure within this reduced dynamical system does not alone establish the global absence of an event horizon in the full spacetime.

9.2.1 Linearized attraction and its domain

For the constant-u baseline, let $y = \varepsilon/x^2$ and $\tau = -\ln x$. Direct differentiation of the scalar evolution equation (144) gives $dy/d\tau = 2y + [(1 - x^2y)/x^2](y^{-1/2} - 1)$, for $x > 0$ and $0 < \varepsilon < 1$. This is an exact transformation, not a new physical equation.

Write $y = 1 + 4x^2 + \delta$, where the $4x^2$ term is the formal leading correction obtained in Equation (138). Linearization about this asymptotic curve yields a dominant perturbation coefficient $-1/(2x^2)$ multiplying δ as $x \to 0$. Thus sufficiently small perturbations about a trajectory already in the small-x regime are strongly damped as τ increases. To leading order the homogeneous perturbation behaves as $\delta \propto \exp[-1/(4x^2)]$ up to subleading factors. This is a local asymptotic statement, not a proof of global attraction from arbitrary initial conditions.

The numerical tests in Tables 1–2 supply finite-domain evidence for selected initial conditions and solver tolerances. Their endpoint $x = x_0/1000$ does not establish convergence for every admissible initial condition or as x reaches zero. Likewise, the power-law-u sensitivity in Section 9.8 concerns the instantaneous balance scaling; it is not an independent perturbation-stability calculation for each variable-u law. A full robustness result would require integration and perturbation tests under those alternative closures and verification of the quasi-static consistency conditions.

9.3 Direction of the restoring tendency

For $0 < \varepsilon < 1$, Equation (134) may be factored as

$$d\varepsilon/ds = (1 - \varepsilon)\sqrt{\varepsilon}(1 - \sqrt{\varepsilon}/x) \tag{140}$$

At fixed instantaneous x, $\varepsilon < x^2$ implies $\sqrt{\varepsilon}/x < 1$ and therefore

$$d\varepsilon/ds > 0 \quad (141)$$

whereas $\varepsilon > x^2$ implies

$$d\varepsilon/ds < 0 \quad (142)$$

Thus the ε component of the vector field points upward below the candidate curve and downward above it. Because x simultaneously decreases, this sign argument identifies a local restoring tendency but is not by itself a global stability proof.

9.4 Evolution with x as the independent variable

Since $dx/ds = -\varepsilon < 0$ for $\varepsilon > 0$, x is monotonic during contraction and may be used as the independent variable. Dividing Equation (134) by Equation (133) gives

$$d\varepsilon/dx = -(1 - \varepsilon)(1/\sqrt{\varepsilon} - 1/x) \quad (143)$$

Equation (143) follows the collapse directly from an initial x to progressively smaller x without integrating over the increasingly long distant-observer time.

9.5 Numerical convergence and sensitivity to initial conditions

We independently reintegrated the constant-u dimensionless system in Equations (133)–(134), using x as a monotonically decreasing coordinate. To reduce the dynamic range, we integrated in $\tau = -\ln x$, for which the equivalent scalar evolution equation is

$$d\varepsilon/d\tau = (1 - \varepsilon)(x/\sqrt{\varepsilon} - 1), \quad \tau = -\ln x \quad (144)$$

This is an exact rewriting of the original ODE for $x > 0$ and $\varepsilon > 0$. Each trajectory was integrated from x_0 to $x_0/1000$ using the implicit Radau integrator. The resulting values are presented in Table 1. The three tolerance pairs (relative, absolute) were $(10^{-7}, 10^{-12})$, $(10^{-9}, 10^{-14})$, and $(10^{-11}, 10^{-16})$. We checked solver success and compared the final ε/x^2 across tolerances. These tolerance comparisons test numerical consistency; they do not constitute a rigorous global error bound.

Table 1. Recomputed trajectories and tolerance comparison. Each entry is the final ratio ε/x^2 at $x = x_0/1000$; digits are displayed only to resolve the comparison.

x_0	ε_0	rtol 10^{-7}	rtol 10^{-9}	rtol 10^{-11}
0.50	0.80	1.000000999151	1.000001000006	1.000001000005
0.50	0.05	1.000000998959	1.000001000006	1.000001000004
0.10	0.50	1.000000032696	1.000000039990	1.000000039998
0.10	0.0001	1.000000020121	1.000000039995	1.000000040000
0.010	0.20	0.999996012515	1.000000001503	1.000000000352
0.010	0.000001	0.999994784957	0.999999999400	1.000000000442

The coarse-tolerance runs show noticeable numerical error for the smallest final radii, while the tighter runs agree increasingly well. At the smallest x, the computed ratio is sensitive to absolute error in ε because ε itself is of order 10^{-10}. Thus a convergence statement should always specify both the tolerance and the radius reached.

Table 2. Additional initial-condition tests, using relative tolerance 10^{-11} and absolute tolerance 10^{-16}. Each entry is the final ratio ε/x^2 at $x = x_0/1000$.

x_0	ε_0	Final ε/x^2
0.80	0.90	1.000002560021
0.80	0.01	1.000002560021
0.30	0.70	1.000000360001
0.30	0.02	1.000000360001
0.030	0.40	1.000000003606
0.030	0.00001	1.000000003579

All twelve tested initial conditions satisfy $0 < \varepsilon_0 < 1$ and $x_0 > 0$, and the numerical integrations reached their designated endpoints. The results are consistent with convergence toward $\varepsilon/x^2 = 1$ from initial conditions above and below the candidate relation. They also agree with the formal leading-order asymptotic prediction $\varepsilon/x^2 = 1 + 4x^2 + O(x^4)$: for example, $x = 0.0005$ predicts a ratio of approximately 1.000001, consistent with the tighter-tolerance results. These experiments establish behavior for the sampled states only, not for all admissible initial conditions or all possible contraction prescriptions.

Numerical Reproducibility:

Numerical environment: Python 3.13.5; SciPy 1.17.0; NumPy 2.3.5. Numerical integration was performed using SciPy's solve_ivp function with the Radau method.

Independent variable $\tau = -\ln x$; state variable ε; derivative $f(\tau, \varepsilon) = (1 - \varepsilon)[(e^{(-\tau)/\sqrt{\varepsilon}} - 1]$. Initial value $\tau_0 = -\ln x_0$; endpoint $\tau f = \tau_0 + \ln(1000)$. No event detection or external forcing was used. Solver success was verified for every reported numerical integration.

Numerical setup for Figures 1 and 2

The six baseline trajectories from Table 1 were integrated using the numerical procedure described above, with relative tolerance ($rtol = 10^{-11}$) and absolute tolerance ($atol = 10^{-16}$). The solid curves show the resulting solutions, and markers identify the starting states.

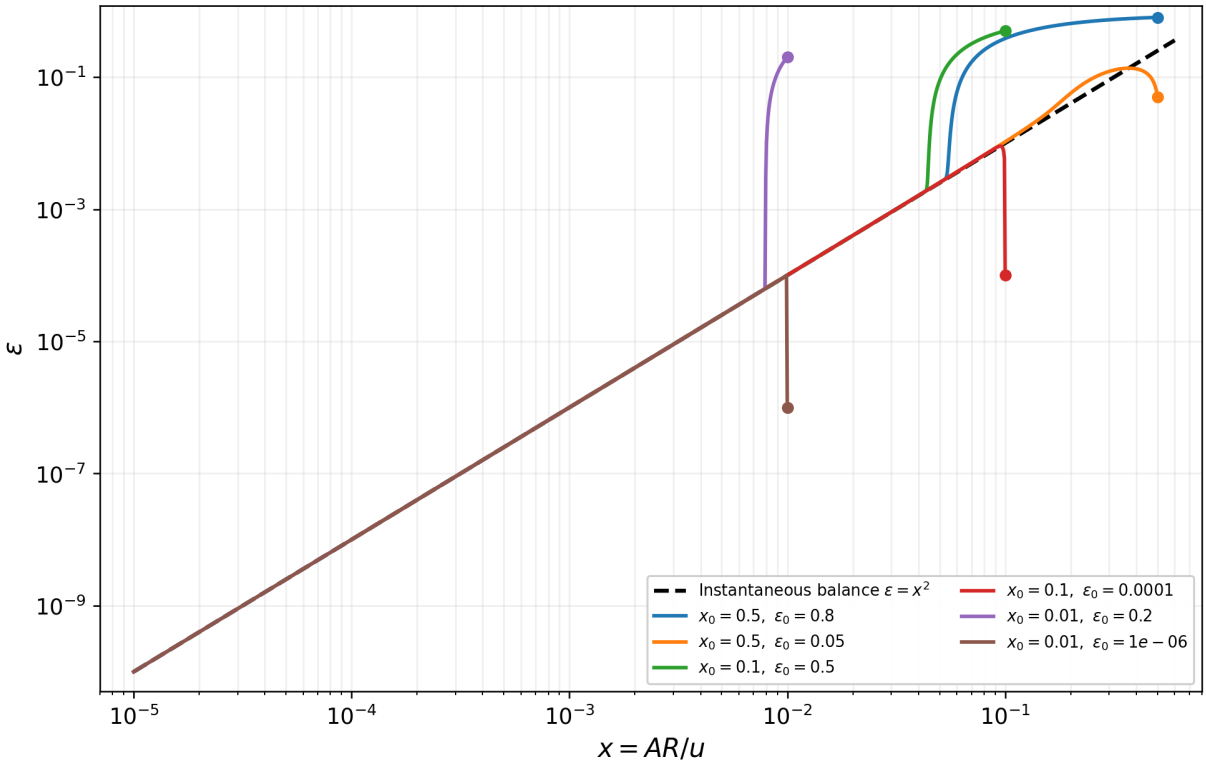


Figure 1. Phase-space trajectories for the six baseline integrations. The dashed curve is $\varepsilon = x^2$. Markers indicate initial states; trajectories approach the small-x balance relation.

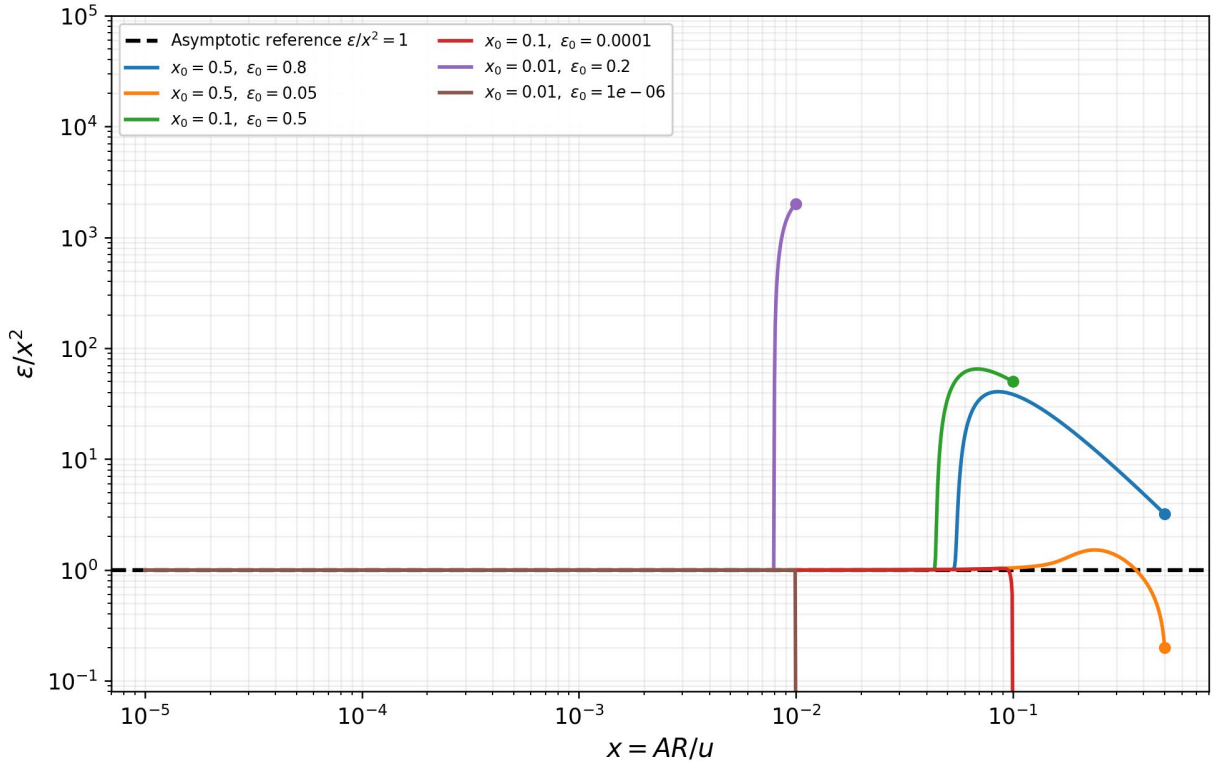


Figure 2. Convergence of ε/x^2 toward unity as x decreases for the same six baseline integrations. The logarithmic vertical scale retains all initial ratios without clipping; the dashed line marks $\varepsilon/x^2 = 1$.

9.5.1 Reproduction protocol, fitted exponents, and numerical diagnostics

Tables 1 and 2 specify all twelve tested initial pairs (x_0, ε_0) and the final ratio ε/x^2 at $x = x_0/1000$. The complete final compactness departure for each entry is recovered without approximation as $\varepsilon_f = (\varepsilon/x^2)_f (x_0/1000)^2$. Figures 1 and 2 display the six baseline phase-space trajectories and their normalized compactness ratios, respectively. Thus the reported tables, plots, and scalar differential equation (144) together specify the finite-domain comparison.

For independent reproduction, integrate the single state ε against $\tau = -\ln x$, with derivative $d\varepsilon/d\tau = (1 - \varepsilon)[\exp(-\tau)/\sqrt{\varepsilon} - 1]$, initial condition $\tau_0 = -\ln x_0$, and endpoint $\tau_f = \tau_0 + \ln(1000)$. The state must remain strictly positive for the square root to be defined. The baseline computations use solve_ivp(method="Radau", rtol=10^{-11}, atol=10^{-16}), without event termination; successful solver status and attainment of τf are required. A convergence comparison repeats the calculation at the two looser tolerance pairs already listed in Table 1. These solver tolerances control local estimated errors and are not certified global error bounds.

To distinguish the exponent from the finite-radius correction, we additionally fitted $\ln \varepsilon$ against $\ln x$ by ordinary least squares at 60 logarithmically spaced sample points per window, evaluating the Radau dense-output solution for the representative initial state $(x_0, \varepsilon_0) = (0.50, 0.80)$. The fitted slopes were 2.006851 over $0.02 \le x \le 0.04$, 2.001689 over $0.01 \le x \le 0.02$, and 2.000421 over $0.005 \le x \le 0.01$. The progressive approach toward exponent 2 agrees with the formal relation $\varepsilon = x^2[1 + 4x^2 + O(x^4)]$. The fit is an empirical finite-window diagnostic, not an independent proof of the limiting exponent.

As an independent numerical rerun using SciPy 1.17.0, the same Radau procedure returned final ε/x^2 = 1.0000010000053 for (x_o, ε_o) = (0.50, 0.80), 1.0000000399997 for (0.10, 0.0001), and 1.0000000003523 for (0.010, 0.20), consistent with the corresponding entries in Table 1 at the displayed precision. Solver success was confirmed for these three runs. The remaining nine initial states and the displayed figures are the previously reported calculations, not additional independent reruns in this check.

The leading asymptotic exponent follows analytically from the reduced evolution equations and the formal expansion in Section 9.2. The finite-range integrations test whether selected trajectories enter that asymptotic regime. Numerical agreement across selected initial conditions, shrinking fitting windows, and solver tolerances does not establish uniform convergence for all admissible data, exact global error bounds, or physical validity beyond the prescribed closure.

9.6 Asymptotic scaling

Once ε/x^2 approaches unity, Equation (133) becomes

$$dx/ds \approx -x^2 \tag{145}$$

Integration gives

$$1/x \approx s + K \tag{146}$$

and therefore, for sufficiently large s,

$$x \propto s^{-1} \tag{147}$$

Because $x = AR/u$ and $s = At_\infty$ for constant A and u,

$$R \propto {t_\infty}^{-1} \tag{148}$$

The compactness departure follows from $\varepsilon \approx x^2$:

$$\varepsilon \propto {t_\infty}^{-2} \tag{149}$$

Since $T_o = \sqrt{\varepsilon}$,

$$T_o \propto {t_\infty}^{-1} \tag{150}$$

and because $1 + z = 1/T_o$,

$$1 + z \propto t_\infty \tag{151}$$

9.7 Mass evolution and infinite distant-observer time

The exact mass-radius relation is

$$M = (Rc^2/2G)(1 - \varepsilon) \tag{152}$$

As $\varepsilon \to 0$,

$$M \approx Rc^2/(2G) \tag{153}$$

so that the baseline radial scaling gives

$$M \propto t_{\infty}^{-1} \tag{154}$$

Solving Equation (146) for s gives

$$s \approx 1/x - K \tag{155}$$

and therefore

$$x \to 0 \Rightarrow s \to \infty \Rightarrow t_{\infty} \to \infty \tag{156}$$

The same limit gives $\varepsilon \to 0$, $T_o \to 0$, and $z \to \infty$. Thus the compactness boundary is approached continuously but is not reached at finite distant-observer time within the baseline coupled model.

9.8 Sensitivity to variable u

Section 8.9 introduced the specified family $u(R) = u_0(R/R_0)^q$. The instantaneous balance then scales as

$$\varepsilon_{bal} \propto R^{(2-2q)} \tag{157}$$

This provides a direct sensitivity test of the constant-u result. Representative choices $q = -0.5$, 0, and +0.5 all satisfy $q < 1$ and therefore retain $\varepsilon \to 0$ as $R \to 0$, but with balance exponents 3, 2, and 1, respectively:

$$q = -0.5: \varepsilon_{bal} \propto R^3 \quad q = 0: \varepsilon_{bal} \propto R^2 \quad q = +0.5: \varepsilon_{bal} \propto R \tag{158}$$

Accordingly, the existence of an asymptotic high-compactness balance within this prescribed family does not depend uniquely on u being constant. What does depend on the contraction prescription is the detailed power-law approach to the limit. The numerical phase-space result $\varepsilon/x^2 \to 1$ applies specifically to the $q = 0$ baseline because $x = AR/u$ is then proportional to R.

For $q = 1$ the balance ε is radius-independent, and for $q > 1$ the balance scaling no longer tends toward zero as R decreases. These cases mark the boundary of the robustness claim and are not represented as ECO-like asymptotic solutions by the present sensitivity argument.

9.9 Comparison with ECO limiting behavior

The baseline TDC solutions share the ECO limiting behavior of increasing redshift, near-unit compactness, and divergent distant-observer evolution time. The coupled dimensionless equations and convergence tests are developed here, not attributed to Mitra.

9.10 Limits of the numerical result

These integrations test the reduced equations, not the physical validity of their spherical, radiative, quasi-static, and contraction assumptions. Rotation, accretion, magnetic fields, or different transport and contraction laws may alter the result.

The numerical attraction is demonstrated for the sampled constant-u initial conditions, not proven globally. The variable-u tests show how the limiting behavior depends on the chosen contraction law.

9.11 Result

For the constant-u baseline, initial states on both sides of $\varepsilon = x^2$ converge numerically toward $\varepsilon/x^2 = 1$ as contraction proceeds. On that attracting relation, $R \propto t_\infty^{-1}$, $M \propto t_\infty^{-1}$, $T_o \propto t_\infty^{-1}$, and $1 + z \propto t_\infty$. The limiting set $R \to 0$, $M \to 0$, $2GM/(Rc^2) \to 1$, and $z \to \infty$ is reached only as $t_\infty \to \infty$. For the specified variable-u family, the balance still approaches $\varepsilon \to 0$ for $q < 1$, although with a modified power-law exponent. These results establish the dynamical behavior of the stated TDC radiative-collapse model and provide the basis for the subsequent ECO-MECO comparison.

10. From ECO to MECO: Magnetic Fields and Observable Compact Objects

Sections 3–9 concerned the gravitational and radiative structure of an eternally collapsing object (ECO). A magnetospheric eternally collapsing object (MECO) adds an intrinsic magnetic moment and a magnetosphere to that ECO core. This distinction is important. The high-redshift, Eddington-supported collapse relations compared with Mitra are ECO results; the detailed magnetic-dipole, disk-interaction, propeller, and jet phenomenology was developed principally by Robertson and Leiter and related collaborators (Robertson & Leiter, 2006) [4]. This section therefore extends the TDC–ECO correspondence to the magnetic case without attributing the full MECO construction to Mitra alone.

10.1 The additional MECO ingredient

The ECO limit established above is characterized by a highly redshifted material surface that remains timelike while approaching the compactness boundary asymptotically. The MECO model adds a persistent intrinsic magnetic moment μ (Robertson & Leiter, 2006). For an approximately dipolar exterior field, the characteristic magnetic-field scaling is

$$B(r) \approx \mu/r^3 \tag{159}$$

where B(r) is the magnetic-field magnitude at areal radius r and μ is the intrinsic magnetic dipole moment. Numerical factors depend on whether the polar or equatorial field is used; the essential point here is the r^{-3} dipolar dependence.

At the compact object's surface R, the corresponding characteristic local field is

$$B_s \approx \mu/R^3 \tag{160}$$

where B_s denotes the locally measured surface magnetic field. The MECO proposal treats the material central compact object itself as the source of an intrinsic magnetic moment.

10.2 Magnetic energy density and equipartition

Robertson and Leiter (2006) describe the MECO interior and atmosphere as a highly redshifted radiating plasma with strong magnetic fields near equipartition and a pair-plasma atmosphere [4]. In Gaussian cgs notation, the local magnetic energy density is

$$u_B = B^2/(8\pi) \tag{161}$$

where u_B is magnetic energy per unit volume. If u_{pl} denotes the characteristic local plasma/radiation energy density, a schematic equipartition condition may be written

$$u_B \approx u_{pl} \tag{162}$$

or

$$B^2/(8\pi) \approx u_{pl} \tag{163}$$

Equations (161)–(158) are standard electromagnetic definitions and a schematic equipartition statement, not a new TDC derivation. Their role is to identify the additional physical sector required to turn an ECO into the magnetospheric MECO proposed in the literature.

10.3 TDC transformation of a surface-generated photon signal

The presence of a magnetosphere does not alter the time-rate mapping already derived for photons escaping from the highly redshifted surface. For any locally generated photon energy E_s, Section 4 gives

$$E_\infty = T_o E_s \tag{164}$$

and the local-to-distant time relation gives

$$d\tau = T_o \, dt_\infty \tag{165}$$

Consequently a surface luminosity generated by thermal, synchrotron, or other local radiative processes transforms as

$$L_\infty = T_o{}^2 L_s \tag{166}$$

where L_s is the locally measured surface luminosity. Thus an intrinsically energetic and magnetically active surface can nevertheless appear extremely faint to a distant observer when T_o is small.

10.4 Magnetic field and redshift must be distinguished

A magnetic field is not a photon luminosity, so Equation (166) should not be applied directly to B itself. The locally measured field B_s and a field inferred by a distant observer depend on the electromagnetic field tensor, geometry, rotation, and the observer's tetrad. Accordingly, the present paper does not assume a universal relation such as $B_\infty = T_o B_s$. Such a relation would require a separate covariant electromagnetic derivation.

What TDC does determine immediately within the adopted time-rate mapping is the redshift of electromagnetic radiation produced by that field. For a locally emitted characteristic synchrotron frequency $\nu_{syn,s}$,

$$\nu_{syn,\infty} = T_o \nu_{syn,s} \tag{167}$$

and similarly for any other locally defined spectral feature. This distinction keeps the gravitational time-rate result separate from assumptions about the detailed magnetic-field geometry.

10.5 Rotating magnetosphere

If the compact object rotates with angular velocity Ω, a dipolar magnetosphere introduces a natural light-cylinder scale. In the usual approximation,

$$R_{LC} = c/\Omega \tag{168}$$

where R_{LC} is the light-cylinder radius. The magnetic field can interact with surrounding plasma and an accretion disk at radii far outside the highly redshifted surface. Robertson and Leiter (2006) use this magnetosphere–disk interaction to model spectral-state changes, magnetic propeller behavior, and jet production in black-hole candidates [4,13].

For an accretion disk with local Keplerian angular frequency

$$\Omega_K(r) = \sqrt{(GM/r^3)} \tag{169}$$

a corotation radius is defined by $\Omega_K(R_c) = \Omega$, giving

$$R_c = \sqrt[3]{(GM/\Omega^2)} \tag{170}$$

Equations (168)–(165) are standard rotating-magnetosphere relations. Their relevance here is that the existence of an intrinsic μ supplies an external physical scale and interaction mechanism absent from the purely radiative ECO equations of Sections 3–9.

10.6 Magnetic pressure at the disk

Using the dipole scaling in Equation (159), the characteristic magnetic pressure at disk radius r is

$$P_B(r) = B^2(r)/(8\pi) \approx \mu^2/(8\pi r^6) \tag{171}$$

A magnetospheric truncation radius can arise where this magnetic stress becomes comparable to the relevant material stress of the inflowing plasma. Schematically,

$$P_B(R_m) \approx P_{flow}(R_m) \tag{172}$$

where R_m is the magnetospheric interaction radius and P_{flow} represents the appropriate ram, gas, radiation, or combined disk stress. The exact R_m relation depends on the accretion model and is therefore not fixed here.

This is another deliberate separation between the present TDC derivation and the detailed Robertson–Leiter MECO model. TDC supplies the compact-object time-rate and redshift structure established in the earlier sections; a full disk–magnetosphere solution requires additional plasma and electromagnetic physics.

10.7 Compatibility of the magnetic extension with the TDC asymptotic ECO

Section 9 found, for the constant-u baseline, the asymptotic relations

$$R \propto t_\infty^{-1}, \quad M \propto t_\infty^{-1} \tag{173}$$

and

$$T_o \propto t_\infty{}^{-1}, \quad 1 + z \propto t_\infty \tag{174}$$

while the compactness tends toward

$$2GM/(Rc^2) \rightarrow 1^- \tag{175}$$

These results describe the gravitational core of the baseline model. Section 9 also showed that the approach toward $\varepsilon \rightarrow 0$ persists for the specified variable-u family when $q < 1$, although its power-law exponent changes. Adding μ does not, by itself, change these gravitational equations unless magnetic energy, pressure, or torque becomes dynamically important in the mass-radius evolution.

A fully self-consistent TDC–MECO solution would therefore supplement the coupled system of Section 8 with electromagnetic contributions to the stress-energy and with an evolution equation for μ or B_s. The present result is consequently one of compatibility rather than a completed magnetohydrodynamic solution.

10.7.1 Separation of derived radiative results and magnetic-plasma assumptions

The results obtained in Sections 3–9 do not require an intrinsic magnetic dipole. Given the shared spherical compactness input, the adopted reciprocal radial prescription, quasi-static Eddington balance, opacity closure, and prescribed contraction speed, the reduced model determines the conditional surface time-rate factor, gravitational redshift, local and distant Eddington luminosities, mass-depletion rate, and asymptotic mass–radius behavior. These are gravitational–radiative results of the stated model; they neither establish the existence of an intrinsic magnetic moment nor determine a magnetic-field strength.

The additional MECO hypothesis is that the central material object maintains a nonzero intrinsic magnetic moment μ and an associated magnetosphere. The dipole scaling in Section 10.1, magnetic energy density and approximate equipartition in Section 10.2, and rotating-magnetosphere and disk-stress relations in Sections 10.5–10.6 are conditional electromagnetic or plasma-model inputs. In particular, the present equations supply no induction or flux-freezing law, conductivity, current distribution, dynamo mechanism, magnetic flux-loss prescription, or evolution equation for μ as M and R decrease. Consequently, a persistent moment, an equipartition pair atmosphere, and any surface-field scaling along the asymptotic trajectory cannot be inferred from the gravitational–radiative solution alone.

Likewise, a light cylinder, corotation radius, magnetic propeller, disk truncation, jet, or polarization signature requires additional specifications of rotation, accretion rate, plasma loading, field topology, and radiative transfer. Their existence or amplitude is not predicted by the spherical TDC baseline. The photon-frequency redshift and conditional surface-luminosity mapping in Sections 10.3–10.4 apply to radiation from a specified emitting region under the adopted static or quasi-static observer transformation; they do not independently predict a synchrotron spectrum or magnetic observable.

Therefore, “compatible with a MECO extension” means only that the reduced ECO-like gravitational–radiative equations do not explicitly exclude adding such a sector when its back-reaction is negligible. If magnetic stresses, electromagnetic radiation, or disk torques materially affect mass loss or contraction, the equations of Sections 8–9 must be rederived with the corresponding stress-energy, angular-momentum balance, and electromagnetic evolution. No self-consistent TDC–MECO solution or observational proof of an intrinsic magnetic moment is claimed here.

10.8 Observable implications of the magnetic extension

Robertson and Leiter applied the MECO magnetosphere to radio/X-ray correlations and jet formation in black-hole candidates and AGN [4,13], and specifically to propeller-driven outflow, broadband emission, flares, and polarization in Sgr A* [14]. Observational evidence interpreted by Schild, Leiter, and Robertson as supporting an intrinsic magnetic moment has also been reported for the central compact object in Q0957+561 [15]. These applications are model-dependent and are not re-derived here.

For the present TDC comparison, the relevant point is narrower: a persistent intrinsic magnetic moment anchored to the central material object would add an observable physical structure not contained in the purely radiative ECO equations. Magnetic fields or jets alone do not establish such an intrinsic moment, because surrounding accretion plasma can itself be strongly magnetized.

10.9 Quantitative Observational Consequences of the Baseline Evolution

The coupled equations of Sections 8–9 yield conditional, quantitative relationships that can be confronted with observations if the surface emission can be isolated and the effective opacity κ and contraction parameter u are independently constrained. These relationships apply to the spherical, quasi-static, Eddington-limited baseline model; they are not universal predictions for arbitrary accreting compact objects.

For constant κ and u, Section 9 gives $\varepsilon \simeq (AR/u)^2$ at small radius, where $A = 4\pi G/(\kappa c)$, $\varepsilon = T_o^2$, and $T_o = 1/(1 + z)$. Thus $T_o \simeq AR/u$ and $1 + z \simeq u/(AR)$. Along a modeled sequence of surface states, the predicted redshift therefore grows inversely with R in the asymptotic regime. The normalization depends on κ and u; without independent estimates of these parameters, the redshift–radius scaling alone does not uniquely identify TDC.

The distant-observer Eddington luminosity derived in Section 6 is $L_\infty = (4\pi GMc/\kappa)T_o$. Combining this relation with the asymptotic compactness condition $M \simeq Rc^2/(2G)$ gives $L_\infty \simeq (2\pi c^3/\kappa)(A/u)R^2$. Consequently, the baseline predicts $L_\infty \propto R^2$, or equivalently $L_\infty \propto (1 + z)^{-2}$, along an asymptotic sequence for which κ and u remain constant. This last proportionality is a dynamical sequence prediction, not the fixed-state photon redshift transformation $L_\infty = T_o^2 L_{loc}$; the local Eddington luminosity itself changes with the evolving state.

The mass-loss equation provides a second consistency relation: $-dM/dt_\infty = L_\infty/c^2 = (4\pi GM/(\kappa c))T_o$. Therefore, the inferred luminosity and rate of gravitational mass loss must agree when measured using the same distant-observer time convention. Simultaneous determinations of surface redshift, luminosity, radius, and mass evolution would overconstrain the baseline assumptions and could falsify this particular closure model.

These expressions are not claimed to distinguish TDC uniquely from all ECO or general-relativistic radiating-surface models. The redshift transformation and Eddington relation are shared with the ECO treatment, while conventional relativistic models with material surfaces may reproduce some of the same scalings. A meaningful discriminant requires a specified competing model, an observable surface component rather than accretion-flow emission, and uncertainty estimates for

κ, u, distance, absorption, and emission geometry. For Sgr A* and other highly accreting sources, those observational separations have not been performed here.

10.9.1 Normalized signal estimates and comparison at matched external conditions

A directly calculable, dimensionless signal in the spherical Eddington-limited model is the ratio of the luminosity received at infinity to the conventional mass-normalized Eddington scale $L_0 = 4\pi GMc/\kappa$. Equations (92) and (108) give $L_\infty/L_0 = T_o = \sqrt{\varepsilon} = 1/(1+z)$. For illustration, $\varepsilon = 10^{-4}$ gives $L_\infty/L_0 = 10^{-2}$ and $z = 99$, whereas $\varepsilon = 10^{-8}$ gives $L_\infty/L_0 = 10^{-4}$ and $z = 9{,}999$. At the same instantaneous M and κ, these are respectively 1% and 0.01% of L_0. These are model-normalized estimates, not predictions of the measured total luminosity of a particular astronomical source.

The corresponding instantaneous gravitational-mass depletion scale is $\tau M = [\kappa c/(4\pi G)]/\sqrt{\varepsilon}$. It is therefore 100 or 10,000 times the reference scale $\kappa c/(4\pi G)$ in the two illustrative cases. This is a depletion timescale rather than a variability or photon-escape delay. In the constant-u asymptotic regime, the integrated time to reach a smaller positive radius is instead governed by the integral in Section 7.7.1. Neither expression specifies a characteristic observed flare duration without an emission and transfer model.

A comparison at fixed mass M, accretion rate $\dot{M}_{acc}$, and viewing geometry must distinguish a surface-origin component from emission by the accretion flow. The present TDC baseline specifies only the conditional Eddington-regulated surface component above. An ideal event-horizon black hole has no material-surface component, but its disk, corona, jet, and surrounding gas may radiate; their luminosities are not predicted by the present equations. A nonzero surface component is therefore a potential difference in physical origin, not a demonstrated difference in the total observed flux at matched $\dot{M}_{acc}$. Moreover, conventional horizonless relativistic surface models can share the same gravitational redshift and Eddington factors, so this ratio alone is not unique to TDC.

For an actual observational comparison, one would need independently constrained M, distance, inclination, $\dot{M}_{acc}$, κ, surface emission spectrum, and photon transport, followed by a forward calculation of flux in specified wavelength bands and its observational upper limits. In particular, a local spectral peak would be redshifted in frequency by T_o under the static-surface approximation, but its observed flux and shape also depend on atmosphere, absorption, lensing, photon escape, and reprocessing. No numerical flux density, color temperature, magnetic field strength, or existing-source exclusion limit can be inferred from the reduced equations alone. The estimates above make the suppression quantitatively explicit while leaving observational discrimination an open test rather than claiming an established detection.

10.10 TDC–ECO–MECO hierarchy

The relationship among the models can therefore be summarized. The TDC compact-object limit developed in this paper satisfies

$$2GM/(Rc^2) < 1 \tag{176}$$

at every finite timelike state, with

$$2GM/(Rc^2) \to 1^- \tag{177}$$

only asymptotically. Under the Eddington-limited conditions of Sections 5–9, this limit reproduces the principal ECO luminosity and lifetime behavior. A MECO then adds

$$\mu \neq 0 \tag{178}$$

together with the associated magnetosphere and its interaction with surrounding plasma. Equation (178) is therefore the defining additional physical ingredient in the hierarchy used here; it is not implied merely by the ECO equations.

10.11 Result

The MECO extension adds an intrinsic magnetic moment and magnetospheric interaction to the TDC–ECO core, but neither the moment nor the associated plasma physics is derived here. The extension is therefore compatible with, rather than established by, the gravitational-radiative calculation [4].

A quantitative magnetic-field prediction requires a covariant electromagnetic and plasma treatment beyond the present model.

11. TDC, ECO/MECO, and the Conventional Black-Hole Interpretation

This section compares the physical interpretations of the models developed in Sections 3–10 without repeating their derivations.

The comparison begins from the shared spherical compactness relation specified in Section 2. From that common input, TDC develops its time-rate, radiative, and coupled dynamical results without adopting Mitra's ECO collapse equations or his disputed no-trapped-surface inference. Agreement between the resulting limiting relations therefore establishes a mathematical correspondence under the stated assumptions, not equivalence of the underlying theories.

Table 3. Comparison of the TDC 10 radiative-collapse model, Mitra ECO, Robertson–Leiter MECO, and conventional general-relativistic black-hole interpretation.

Feature	**TDC 10 (present model)**	**Mitra ECO**	**Robertson–Leiter MECO**	**Conventional GR black-hole interpretation**
Framework	TDC time-rate prescription applied to spherical radiative collapse; conditional coupled mass–radius evolution.	Proposed radiating, continually collapsing material object within a GR-based treatment.	ECO-like central object supplemented by intrinsic magnetism and plasma physics.	GR permits black-hole solutions and horizon formation under appropriate collapse conditions; not a single matter or emission model.
Central surface / horizon	Material, timelike surface remains outside the compactness limit along the modeled	Proposed timelike material surface approaching extreme compactness	Proposed material central object without an event horizon, with a magnetosphere.	An event horizon is a causal boundary, not a material surface; realistic collapse depends on stress–

	trajectories; no global no-horizon theorem established.	without a trapped surface; general validity disputed.		energy and initial data.
Radiation / mass loss	Assumes quasi-static Eddington-regulated surface radiation, prescribed opacity and contraction; derives distant luminosity and coupled mass loss.	Radiation pressure and gravitational redshift are central to the ECO picture.	Includes radiation plus pair-plasma atmosphere and magnetospheric processes.	Emission may arise from accretion and surrounding plasma; radiation from matter before horizon formation is also possible.
Surface redshift	$1 + z = 1/T_o$ under the adopted spherical compactness mapping; increases along the asymptotic branch.	Very large surface redshift as the proposed object continues to contract.	Extreme central-object redshift, together with magnetospheric emission.	Redshift of photons emitted outside the horizon can become arbitrarily large as emission approaches it; no stationary material surface at the horizon.
Magnetic / plasma physics	No intrinsic magnetic moment or plasma dynamics derived by the present gravitational–radiative equations.	Intrinsic magnetic structure is not required for the basic ECO proposal.	Postulates intrinsic magnetic moment, magnetosphere, pair plasma, and disk coupling.	Magnetized accretion flows and jets can exist around black holes without a central intrinsic magnetic moment.
Potential discrimination	Quantify time-dependent redshift, distant luminosity, mass–radius evolution, and deviations from the prescribed asymptotic law; shared scalings are not unique evidence.	Search for consequences of a persistent, highly redshifted material surface, with realistic radiative transfer.	Test whether observations require a persistent magnetic moment anchored to the central object rather than the accretion flow.	Compare predictions for accretion, compact emission, and gravitational waves against well-specified alternatives; many signatures overlap.

The table distinguishes the conditional TDC 10 model from ECO and MECO proposals and from general relativity as a broader theory. The shared compactness, redshift, and luminosity relations

do not by themselves distinguish these descriptions. A decisive test requires quantitative predictions incorporating the relevant surface, accretion, radiation-transfer, and plasma physics.

11.1 Conventional event-horizon description

In the conventional general-relativistic interpretation, a nonrotating, uncharged Schwarzschild black hole contains an event horizon at

$$R_S = \frac{2GM}{c^2} \tag{179}$$

corresponding to compactness $2GM/(Rc^2) = 1$. An event horizon is a causal boundary rather than a material surface; signals originating inside it do not reach future null infinity.

Observable radiation, magnetic fields, jets, and accretion signatures outside a conventional black hole are therefore modeled through the exterior spacetime and surrounding plasma. Consequently, a dark compact region, strong gravitational redshift, relativistic accretion, magnetic fields, or jets does not by itself distinguish an event-horizon model from a sufficiently compact horizonless model.

11.2 The TDC–ECO distinction

The TDC finite-state condition was derived in Section 3. Every finite timelike state satisfies

$$T_o > 0, \quad \frac{2GM}{Rc^2} < 1 \tag{180}$$

while the limiting sequence is

$$T_o \to 0^+, \quad z \to \infty, \quad \frac{2GM}{Rc^2} \to 1^- \tag{181}$$

Thus the physical distinction is not the limiting compactness itself, but whether that value is reached as an event horizon or approached asymptotically by a timelike material object. In the constant-u baseline of Sections 8–9, the TDC limit is approached only as $t_\infty \to \infty$. The variable-u analysis preserves the approach toward $\varepsilon \to 0$ for the specified family with $q < 1$, although the asymptotic exponent changes.

The redshift, Eddington luminosity, luminosity suppression, and depletion-timescale relations supporting this result have already been derived in Sections 4–7 and are not repeated here.

11.3 The additional MECO distinction

An ECO need not possess the full magnetic structure of a MECO. As discussed in Section 10, the Robertson–Leiter MECO model adds a persistent intrinsic magnetic moment,

$$\mu \neq 0 \tag{182}$$

and an associated magnetosphere capable of interacting with surrounding plasma [4,13,14,15].

This magnetic extension provides a possible observational distinction, but magnetic fields, polarization, or jets alone are insufficient because conventional accretion flows can also be strongly

magnetized. The more discriminating question is whether observations require a persistent intrinsic magnetic moment anchored to the central compact object rather than magnetic fields generated in the surrounding accretion flow.

11.4 Surface radiation and observational appearance

The TDC–ECO object remains material and timelike at every finite stage and can therefore possess locally generated surface radiation. Sections 4–6 showed, however, that photon energy and arrival rate are increasingly suppressed for a distant observer as T_o decreases. For the Eddington-supported sequence, the observed luminosity tends toward zero in proportion to T_o.

Consequently, the existence of a material surface does not imply an easily detectable surface spectrum at extreme compactness. Any proposed observational surface test must include the predicted gravitational redshift, time dilation, and radiative-transfer effects rather than assume an unsuppressed local spectrum.

11.5 Potential observational discriminants

The most useful tests are therefore observations for which a material-surface or intrinsic-magnetosphere model and an event-horizon model make quantitatively different predictions. Two broad possibilities follow from the present comparison.

First, evidence requiring a persistent intrinsic magnetic moment anchored to the central object would support the MECO magnetic extension, whereas magnetic fields attributable to the surrounding plasma would not discriminate between the models.

Second, evidence of a material emitting region at extreme compactness could test the TDC–ECO interpretation, provided that the predicted redshift and luminosity suppression are included quantitatively.

Observations of orbital dynamics, relativistic accretion, compact emission regions, gravitational waves, magnetic fields, or jets remain important tests of compact-object environments, but none alone establishes either an event horizon or a TDC–ECO/MECO central structure.

11.6 Falsifiability and scope

The TDC compact-object interpretation imposes a definite finite-state condition. Within the model developed here, a finite timelike state with

$$\frac{2GM}{Rc^2} \geq 1 \tag{183}$$

would contradict that domain. Likewise, observations inconsistent with the coupled asymptotic behavior under the physical conditions to which the model is claimed to apply would challenge that application.

The MECO extension is separately testable. Demonstrating that a proposed MECO signature can be fully accounted for by accretion-generated magnetism would remove that observation as evidence for an intrinsic central magnetic moment. Conversely, establishing an intrinsic central moment

would support a material magnetospheric interpretation without, by itself, establishing the complete TDC framework.

11.7 Result

The descriptions may share exterior observational features, but differ in their proposed central structure: an event horizon in conventional black-hole models, a timelike asymptotically collapsing surface in the present TDC–ECO solution, and an added intrinsic magnetosphere in MECO.

Discriminating among them requires quantitative evidence for a horizon, a material surface, or an intrinsic central magnetic field—not compactness or faintness alone.

12. Physical Implications and Scope of the TDC Compact-Object Solution

Sections 3–9 established the TDC–ECO correspondence and the coupled mass–radius evolution. This section considers the physical implications and limits of those results.

The correspondence remains conditional on the common spherical compactness input and the model assumptions identified above.

12.1 A continuously evolving material compact object

The modeled surface remains timelike at each finite stage while its time-rate factor decreases and its redshift increases toward the asymptotic limit.

For the constant-u baseline tested numerically in Section 9, the attracting relation is

$$\frac{\varepsilon}{x^2} \to 1 \tag{184}$$

with the asymptotic scalings

$$R(t_\infty) \propto {t_\infty}^{-1}, M(t_\infty) \propto {t_\infty}^{-1}, T_o(t_\infty) \propto {t_\infty}^{-1}, \; 1 + z(t_\infty) \propto t_\infty \tag{185}$$

These scalings describe the dynamical result, not merely the static ECO compactness relation.

12.2 Local evolution versus distant appearance

Sections 4–6 show that the local photon energy and the arrival rate measured at infinity are each reduced by the time-rate factor T_o.

A locally radiating material surface can therefore become progressively faint to a distant observer; faintness alone does not establish that no surface exists.

The same distinction may have a further geometrical consequence for the spacetime-vortex interpretation developed in earlier TDC work. Because the local time rate approaches zero while the continuum remains dynamically evolving, the apparent radial depth of the compact-object vortex need not represent a fixed, observer-independent spatial dimension. The reciprocal temporal-spatial scaling derived in Section 2 suggests instead that the perceived depth may depend upon the observer's position and time-rate frame within the gradient. A complete treatment would require extension of the present spherical solution to the three-dimensional FDE/GDE vortex geometry and is reserved for subsequent work.

12.3 Mass loss and asymptotic collapse

Section 7 gives an instantaneous depletion timescale proportional to 1 + z. Sections 8–9 extend this relation by evolving M, R, and T_o together.

The resulting object continues to contract and lose mass, with rates that diminish in distant-observer time.

12.4 Dependence on the contraction prescription

The detailed constant-u power laws are not universal consequences of the TDC time-rate field. Section 8 therefore introduced the specified sensitivity family

$$u(R) = u_0 \left(\frac{R}{R_0}\right)^q \tag{186}$$

For this family, the instantaneous high-compactness balance scales as

$$\varepsilon_{\mathrm{bal}} \propto R^{2-2q} \tag{187}$$

Thus the balance continues toward $\varepsilon \to 0$ for $q < 1$, remains radius-independent for $q = 1$, and reverses its small-R trend for $q > 1$. The specific t_∞^{-1} scalings demonstrated numerically therefore belong to the constant-u baseline; the broader result is the existence of an asymptotic high-compactness regime over the stated range of the specified contraction family.

12.5 Relation to ECO and MECO

The ECO correspondence concerns the radiating, asymptotically collapsing material core, derived here without Mitra's disputed Γ–V inference [2,3].

As Section 10 explains, MECO adds magnetic and plasma assumptions that are not consequences of the present gravitational-radiative equations [4,13,14,15].

12.6 What the calculation establishes—and what it does not

The coupled equations yield an asymptotic attracting relation for the initial conditions numerically tested in Section 9; this extends the static TDC–ECO correspondence.

These results neither prove the absence of trapped surfaces in general relativity nor establish a global attractor for arbitrary collapse histories.

Their applicability depends on the stated spherical, quasi-static, Eddington-limited model and its contraction prescription; more complete radiation, accretion, rotation, and magnetic dynamics remain to be tested.

12.7 New testable content

The model-specific quantitative result is the constant-u approach toward $\varepsilon/x^2 = 1$, together with the sensitivity of the limiting balance to the prescribed radial dependence of u.

Further tests should relax the constant-opacity, constant-contraction, spherical, and nonmagnetic assumptions and assess whether the predicted scaling survives.

12.7.1 Scope of possible quantum-gravitational extensions

The present analysis concerns macroscopic, spherically symmetric gravitational collapse and the evolution of a radiating material surface. Its principal variables—gravitational mass, areal radius, local time-rate factor, compactness departure, and contraction speed—describe the classical gravitational and radiative behavior of the modeled object.

Quantum and semiclassical treatments address additional phenomena, including Hawking radiation, quantum particle production, possible microscopic black-hole states, and quantum corrections to classical gravitational collapse. Depending on the theoretical framework, such approaches may also investigate black-hole entropy, singularity resolution, and the microscopic structure of spacetime. These results cannot be derived from the classical equations developed in TDC 10.

The advantage of the present TDC formulation is its comparatively simple mathematical treatment of macroscopic collapse through directly related time-rate, mass-loss, and contraction variables. It permits explicit examination of the asymptotic compactness limit and the evolution of gravitational redshift without introducing a quantum-gravitational model. This simplicity does not establish greater physical precision than quantum-based approaches, nor does it replace their predictions.

Although TDC may eventually be extended to microscopic scales, the present equations do not establish quantum-scale black holes, elementary-particle structure, or cosmological creation mechanisms. Such extensions would require additional physical assumptions, quantum or semiclassical dynamics, and independently testable quantitative predictions.

Accordingly, the conclusions of TDC 10 remain restricted to the specified macroscopic gravitational model and its radiative and contraction assumptions.

13. Conclusions

This paper compared TDC with the principal ECO relations using an explicitly shared spherical compactness input, then extended the comparison to coupled mass–radius evolution without adopting Mitra's disputed no-trapped-surface inference [2,3].

The model-specific contribution is the dynamical behavior analyzed in Sections 8–9.

13.1 Principal TDC–ECO correspondence

For every finite timelike state admitted by the TDC compact-object model,

$$T_o > 0, \quad \frac{2GM}{Rc^2} < 1 \tag{188}$$

while the limiting sequence is

$$T_o \to 0^+, \quad z \to \infty, \quad \frac{2GM}{Rc^2} \to 1^- \tag{189}$$

The TDC force-gradient and radiative derivations then reproduce the corresponding ECO local Eddington enhancement, two-factor luminosity suppression at infinity, and divergent distant-observer depletion timescale derived in Sections 5–7. These relations are consequences of the TDC treatment of the shared compactness input and should not be interpreted as an independent derivation of that input itself.

13.2 Coupled dynamical result

The principal new result arises when gravitational mass and radius are allowed to evolve simultaneously. For the constant-u baseline, the numerical integrations from initial states on both sides of the candidate balance relation converge toward

$$\frac{\varepsilon}{x^2} \rightarrow 1 \tag{190}$$

with the asymptotic behavior

$$R(t_\infty) \propto {t_\infty}^{-1}, M(t_\infty) \propto {t_\infty}^{-1}, T_o(t_\infty) \propto {t_\infty}^{-1}, \ 1 + z(t_\infty) \propto t_\infty \tag{191}$$

Thus the ECO-like high-redshift state appears as an attracting asymptotic relation of the tested coupled TDC equations rather than as an imposed exact compactness condition.

The sensitivity analysis shows that the detailed power law depends on the contraction prescription. For

$$u(R) = u_0 \left(\frac{R}{R_0}\right)^q \tag{192}$$

the high-compactness balance tends toward $\varepsilon \rightarrow 0$ for the specified family with $q < 1$; $q = 1$ produces a radius-independent balance, while $q > 1$ reverses the small-R trend. The t_∞^{-1} scaling is therefore a result of the constant-u baseline rather than a universal TDC collapse law.

13.3 Physical interpretation and scope

The model describes a material surface that remains timelike at each finite stage while becoming increasingly redshifted to a distant observer. This differs from the conventional event-horizon interpretation.

Neither the ECO correspondence nor the numerical trajectories establish a general prohibition on trapped surfaces; the intrinsic magnetic sector of MECO also remains outside the present derivation [4,13,14,15].

The predictions remain conditional on the radiative, geometric, and contraction assumptions stated in Sections 7–9.

13.4 Final conclusion

TDC 10 reproduces the principal ECO limiting relations after adopting the shared spherical compactness factor and develops a coupled dynamical model whose tested trajectories approach an asymptotically collapsing, increasingly redshifted state.

For constant u, ε/x^2 approaches unity and R, M, and T_o scale approximately as t_∞^{-1}; the variable-u sensitivity demonstrates that the detailed scaling depends on the contraction prescription.

The resulting conditional prediction offers a quantitative target for further physical and observational tests.

Acknowledgment

The author acknowledges the assistance of OpenAI's ChatGPT (GPT-5.6 Sol) in the preparation of this manuscript. ChatGPT was used as an editorial and analytical aid in reviewing mathematical consistency, checking derivational steps and notation, improving clarity and organization, and assisting with manuscript preparation. The theoretical framework, physical interpretations, derivations, conclusions, and final responsibility for the content are solely those of the author.

References

[1] Forrington, Capt. J. H. (Cass) (2024) The Unified Field. *Journal of Modern Physics,* Vol.15, No. 7, 27 June 2024. DOI: 10.4236/jmp.2024.157043

[2] Mitra, A. (2002). On the Final State of Spherical Gravitational Collapse. Foundations of Physics Letters, 15, 439–471. DOI: 10.1023/A:1023968113757.

[3] Mitra, A. (2006). Radiation Pressure Supported Stars in Einstein Gravity: Eternally Collapsing Objects. Monthly Notices of the Royal Astronomical Society, 369, 492–496. DOI: 10.1111/j.1365-2966.2006.10332.x.

[4] Robertson, S. L., & Leiter, D. J. (2006). The Magnetospheric Eternally Collapsing Object (MECO) Model of Galactic Black Hole Candidates and Active Galactic Nuclei. In P. V. Kreitler (Ed.), New Developments in Black Hole Research (pp. 1–44). Nova Science Publishers. arXiv:astro-ph/0602453.

[5] Forrington, Capt. J. H. (Cass) (2025). Time Dilation Cosmology 5: Dimensionality and Spatial Expansion and Contraction in the Holographic Spacetime Continuum. Journal of Cosmology, Vol. 20, 8860–8879, 07 July 2025. https://thejournalofcosmology.com/TDC5JoC.pdf

[6] Oppenheimer, J. R., & Snyder, H. (1939). On Continued Gravitational Contraction. Physical Review, 56, 455–459. DOI: 10.1103/PhysRev.56.455.

[7] Penrose, R. (1965). Gravitational Collapse and Space-Time Singularities. Physical Review Letters, 14, 57–59. DOI: 10.1103/PhysRevLett.14.57.

[8] Mazur, P. O., & Mottola, E. (2004). Gravitational Vacuum Condensate Stars. Proceedings of the National Academy of Sciences, 101, 9545–9550. DOI: 10.1073/pnas.0402717101.

[9] Vaidya, P. C. (1951). The Gravitational Field of a Radiating Star. Proceedings of the Indian Academy of Sciences, Section A, 33(5), 264–276. DOI: 10.1007/BF03173260.

[10] Misner, C. W., & Sharp, D. H. (1964). Relativistic Equations for Adiabatic, Spherically Symmetric Gravitational Collapse. Physical Review, 136(2B), B571–B576. DOI: 10.1103/PhysRev.136.B571.

[11] Israel, W. (1966). Singular Hypersurfaces and Thin Shells in General Relativity. Il Nuovo Cimento B, 44(1), 1–14. DOI: 10.1007/BF02710419.

[12] Santos, N. O. (1985). Non-Adiabatic Radiating Collapse. Monthly Notices of the Royal Astronomical Society, 216(2), 403–410. DOI: 10.1093/mnras/216.2.403.

[13] Robertson, S. L., & Leiter, D. J. (2004). On the Origin of the Universal Radio–X-Ray Luminosity Correlation in Black Hole Candidates. Monthly Notices of the Royal Astronomical Society, 350, 1391–1396. DOI: 10.1111/j.1365-2966.2004.07741.x. arXiv:astro-ph/0402445.

[14] Robertson, S. L., & Leiter, D. J. (2006). Does Sgr A* Have an Intrinsic Magnetic Moment Instead of an Event Horizon? arXiv:astro-ph/0603746.

[15] Schild, R. E., Leiter, D. J., & Robertson, S. L. (2006). Observations Supporting the Existence of an Intrinsic Magnetic Moment inside the Central Compact Object within the Quasar Q0957+561. The Astronomical Journal, 132(1), 420–432. DOI: 10.1086/504898. arXiv:astro-ph/0505518.